PHOTOCATALYTIC CONVERSION OF CARBON DIOXIDE TO ALCOHOLS OVER TITANIUM DIOXIDE-GRAPHENE COMPOSITE

KRITTAMET YANAWIBUT

A THESIS SUBMITTED IN PARTIAL FULFILLMENT
OF THE REQUIREMENT FOR
THE DEGREE OF MASTER OF ENGINEERING
(CHEMICAL ENGINEERING)
FACULTY OF GRADUATE STUDIES
MAHIDOL UNIVERSITY
2017

Thesis
entitled

PHOTOCATALYTIC CONVERSION OF CARBON DIOXIDE TO ALCOHOLS OVER TITANIUM DIOXIDE-GRAPHENE COMPOSITE

.....

Mr. Krittamet Yanawibut
Candidate

.....

Asst. Prof. Pattaraporn Kim-Lohsoontorn,
Ph.D. (Earth Science and Engineering)
Major advisor

.....

Mr. Sira Srinives,
Ph.D. (Chemical and Environmental Engineering)
Co-advisor

.....

Prof. Patcharee Lertrit,
M.D., Ph.D. (Biochemistry)
Dean
Faculty of Graduate Studies
Mahidol University

.....

Asst. Prof. Chularat (Krongtaew) Sakdaronnarong,
Ph.D. (Chemical Engineering)
Program Director
Master of Engineering Program in Chemical Engineering
Faculty of Engineering,
Mahidol University

Thesis
entitled

PHOTOCATALYTIC CONVERSION OF CARBON DIOXIDE TO ALCOHOLS OVER TITANIUM DIOXIDE-GRAPHENE COMPOSITE

was submitted to the Faculty of Graduate Studies, Mahidol University
for the degree of Master of Engineering (Chemical Engineering)
on
March 29, 2017

.....
Mr. Krittamet Yanawibut
Candidate

.....
Miss Mutsee Termtanun,
Ph.D. (Chemical and Environmental Engineering)
Chair

.....
Asst. Prof. Pattaraporn Kim-Lohsoontorn,
Ph.D. (Earth Science and Engineering)
Member

.....
Asst. Prof. Chularat (Krongtaew) Sakdaronnarong,
Ph.D. (Chemical Engineering)
Member

.....
Mr. Sira Srinives,
Ph.D. (Chemical and Environmental Engineering)
Member

.....
Prof. Patcharee Lertrit,
M.D., Ph.D. (Biochemistry)
Dean
Faculty of Graduate Studies
Mahidol University

.....
Asst. Prof. Jackrit Suthakorn,
Ph.D. (Biomedical Engineering)
Dean
Faculty of Engineering,
Mahidol University

ACKNOWLEDGEMENTS

The acknowledgement is made to Thailand Research Fund (TRF) and Research University Network (RUN) for supporting this research. The author would like to extend his sincere gratitude to Asst. Prof. Pattaraporn Kim-Lohsoontorn and Dr. Sira Srinives for them guidance and support throughout the process. My sincere gratitude would also go to keen researchers at Encon-LAB and NANOCEN, staffs from Dept. of Chemical Engineering, and Chemical Engineering faculties for their friendship, support and kind hospitality.

Krittamet Yanawibut

PHOTOCATALYTIC CONVERSION OF CARBON DIOXIDE TO ALCOHOLS OVER TITANIUM DIOXIDE-GRAPHENE COMPOSITE

KRITTAMET YANAWIBUT 5837432 EGCH/M

M.Eng. (CHEMICAL ENGINEERING)

THESIS ADVISORY COMMITTEE: PATTARAPORN KIM-LOHSOONTORN, Ph.D., SIRA SRINIVES, Ph.D.

ABSTRACT

Photo-catalyst comprising titanium dioxide-reduced graphene oxide (TiO_2/rGO) and copper(II)oxide-titanium dioxide-reduced graphene oxide (CuO-TiO_2/rGO) were developed for CO_2 conversion to ethanol. The effects of TiO_2 (10-60 wt.%)and CuO contents (0.3-2.0 wt.%), type of titanium source (sol-gel and P25), and different synthesis methods (sol-gel and sol-gel with heat treatment) were investigated. The most suitable condition reported in this study included the synthesis of 0.5wt.%CuO-20wt.%TiO_2/rGO using 12 hour-stirring with sol-gel with heat treatment method. The highest recorded ethanol yield was obtained at 162.67 $\mu mol/g_{catalyst}$ (100 ml min^{-1} CO_2, 12 hours, 160 W mercury lamp).

KEY WORDS: GRAPHENE/ TITANIUM DIOXIDE/ PHOTOCATALYTIC CONVERSION/ CARBON DIOXIDE UTILIZATION

71 pages

การใช้วัสดุเชิงประกอบไทเทเนียมไดออกไซด์แกรฟีนในการเร่งปฏิกิริยาด้วยแสงเพื่อเปลี่ยนคาร์บอนไดออกไซด์เป็นแอลกอฮอล์

PHOTOCATALYTIC CONVERSION OF CARBON DIOXIDE TO ALCOHOLS OVER TITANIUM DIOXIDE-GRAPHENE COMPOSITE

กฤตเมธ ยานะวิบุตร 5837432 EGCH/M

วศ.ม. (วิศวกรรมเคมี)

คณะกรรมการที่ปรึกษาวิทยานิพนธ์: ภัทรพร คิม , Ph.D., ศิระ ศรีนิเวศน์ , Ph.D.

บทคัดย่อ

งานวิจัยนี้ได้ทำการสังเคราะห์วัสดุเชิงประกอบร่วมที่มีองค์ประกอบระหว่างวัสดุคอปเปอร์(II)ออกไซด์และไทเทเนียมไดออกไซด์บนแกรฟีนที่มีขนาดระดับนาโนเพื่อเป็นตัวเร่งปฏิกิริยาที่ใช้แสงในการเปลี่ยนรูปก๊าซคาร์บอนไดออกไซด์เป็นสารละลายเอทานอลในสภาวะของเหลว โดยศึกษาปริมาณของไทเทเนียมออกไซด์(10-60wt.%)และคอปเปอร์(II)ออกไซด์(0.3-2.0wt.%)บนวัสดุแกรฟีน ร่วมถึงชนิดของไทเทเนียมไดออกไซด์(โซลเจลและP25) และกระบวนการสังเคราะห์โซลเจลและโซลเจลอุณหภูมิสูง) โดยที่ CuO-TiO_2/rGO (0.5%wt CuO, 20%wt TiO_2)ที่สังเคราะห์จากกระบวนการโซลเจลอุณหภูมิสูง สามารถเปลี่ยนรูปก๊าซคาร์บอนไดออกไซด์เป็นสารละลายเอทานอลสูงสุดถึง 162.67 ไมโครโมลต่อกรัมของตัวเร่งปฏิกิริยาโดยใช้เวลาในการทำปฏิกิริยา 12 ชั่วโมง ที่อัตราการไหลของก๊าซคาร์บอนไดออกไซด์ 100 มิลลิลิตรต่อนาทีและใช้หลอดไอปรอท 160 วัตต์เป็นแหล่งกำเนิดแสง

71 หน้า

CONTENTS

CONTENTS (cont.)

LIST OF TABLES

LIST OF FIGURES

LIST OF FIGURES (cont.)

LIST OF FIGURES (cont.)

LIST OF FIGURES (cont.)

CHAPTER I
INTRODUCTION

1.1Rational

Global warming is one of the serious most issue, involving formation of heat trapping layers in atmosphere that consist of potential greenhouse gases, such as methane, nitrous oxide and carbon dioxide. According to a study from zfacts [1], concentration of CO_2 in tropospheric atmosphere has increased from 300 ppm in 1990 to 375 ppm in 2004, as resulted from industrial revolution and combustion of fossil fuel [2]. General approach in coping with CO_2 relies mainly on gas absorption technique, utilizing acid-base reactions between CO_2 and amine solution or alkaline carbonates. Although the approach is effective with maturity of related, it generates liquid/solid waste that requires further treatment. On the other hand, groups of researcher have paid a great deal of attention in developing a breakthrough technology that catalytically converts CO_2 to other chemical compounds, such as hydrogen (H_2), methane (CH_4), ethane (C_2H_4) and methanol, which can be used as energy source.

CO_2 can normally be transformed to dry ice and organic compound, and utilized as syngas, in generating electricity. Several researches work demonstrated uses of photocatalyst for a conversion of CO_2 to other form of energy fuels, such as methane and methanol. This would not only get rid of CO_2 from industrial effluent gas streams, but also yield energy sources – killing two birds with one stone. However, catalytic conversion of CO_2 to other fuel gases, such as methane and hydrogen are not very practical as the gases provide low energy content (per mole) and are difficult to manage. Liquid fuel, such as alcohols, with higher energy content and easier to manage, is preferred [2, 3].

Photocataytic conversion of CO_2 to fuels mainly relies on photocatalyst, such as ZnO and TiO_2, in reforming CO_2 molecules to hydrocarbon substances, such as methane, methanol and ethanol. However, TiO_2 nanoparticles, along with other nanoparticles, would suffer from particle agglomeration, reducing their active surface area and catalytic activity. In 2014, Li K. and his team demonstrated that CO_2 can be

converted to other forms of product- methane, methanol and ethanol [4]. The TiO_2 particles can be synthesized, based onhydrolysis reaction of titanium alkoxide, followed by an annealing process in presence of oxygen. Crystallography of the material governs molecular structures that lead to energy band gap. Photocatalytic activity of TiO_2 can be enhanced by modifying TiO_2 with other metals, such as platinum, gold, silver, zinc, and copper [5-7]. The metal ions enhance rate of photocatalytic oxidation or reduction by changing the dynamics of electron–hole recombination and interfacial charge transfer. The metal-doped TiO_2 is noted as a potential catalyst for CO_2 conversion, and is targeted as our aim of study.Copper is a semiconductor and can also be mildly activated by visible light. Many researchers studied photocatalytic reaction of CO_2 in alkaline solution at liquid/solid interface of copper-doped titanium dioxide bimetallic catalyst, and suggested that copper in state of cupric oxide (CuO) was required in methanol production. It was noted that the CuO acted as free electron collector, converting Cu^{2+} to Cu^{+} [5]. The Cu^{+} can further donate electron to proton from water, transforming back to Cu^{2+}.

Graphene is a 2-dimensional nanostructure with outstanding charge transportation, mechanical strength, and chemical stability properties. It can be synthesized in gram scale using chemical exfoliation path, also known as Hummers' method [8], relying on chemical oxidation of graphite and potassium permanganate. The oxidized state of graphite, graphene oxide (GO), contains C-H-O functional groups, such as carboxyl, carbonyl, and epoxy, that provide electrostatic charges to attract cation from the aqueous solution, and allow metal/metal oxide site specific deposition. By using chemical synthesis approach, e.g. sol-gel method, TiO_2 nanoparticles can be created and immediately immobilized on graphene supports, becoming TiO_2/GO composite in one step. After that, thermal process was used to partially reduce functional groups from GO, producing reduced graphene oxide (rGO) [9].

In this work, CuO-TiO_2/rGO composite was synthesized, following sol-gel method, and demonstrated for photocatalytic conversion of CO_2 to liquid fuel. The composite was uniformly dispersed in DI water and activated under UV-visible light from a mercury lamp while CO_2 gas was purged in. The solution was periodically sampled, and chromatographically tested for liquid fuel contents

1.2 Objectives

1.2.1 To synthesize metal/metal oxide-graphene composites and characterize for their chemical, physical, crystallographic properties.

1.2.2 To test photocatalytic performances of the composites in converting CO_2 to liquid fuels.

1.2.3 To observe effects of operation parameters, such as amount of catalyst and metal/metal oxide, graphene ratio, and liquid fuel production.

1.3 Scopes of study

1.3.1 Synthesizing graphene, following chemical exfoliation method.

1.3.2 Compositing graphene with metal oxide on TiO_2/rGO composite and varying %wt of TiO_2 from 10 to 60%wt.

1.3.3 Investigating effects of doping Cu on TiO_2/rGO composite with several amount of Cu %wt loading (0.5 to 2%wt).

1.3.4 Converting CO_2 into ethanol fuel from in an aqueous solution.

CHAPTER II
THEORY AND LITERATURE REVIEW

2.1 Carbon dioxide (CO_2)

2.1.1 Hazard of CO_2

Fossil fuel, including coal, gasoline, and natural gas, are main sources of energy, relies on combustion reaction to create heat and exhausted gases. On the other hand, the revolution back fired deterioration in environmental conditions, air quality, or even biological system in general. One main drawback is an emission of carbon dioxide (CO_2) due to fossil fuel combustion in transportation, and industries that leads to global warming, affecting environmental conditions. Different CO_2 concentration limits were enacted worldwide, hoping to cope with the issue (Table 2.1 [10]). Although CO_2 is relatively stable compound with low hazard level (TWA value of 5,000 ppm.), its long-term effects have not been well explored.

Table 2.1 Exposure limits for CO_2: 8-hour Time-Weighted Average (TWA) of 5,000 ppm, and 15-minute Short-Term Exposure Limit (STEL) [10]

Standard/Country	8-hour Time- Weighted Average	15-minute Short-Term Exposure Limit
United Kingdom WEL	5,000 ppm	15,000 ppm
USA NIOSH REL	5,000 ppm	30,000 ppm
USA OSHA PEL	5,000 ppm	None listed
ACGIH® TLV®	5,000 ppm	30,000 ppm

Exposure to such a high concentration of CO_2 cause headache, dizziness, difficulty in breathing, nauseas, and depression of nervous system. The National Institute for Occupational Safety and Health (NIOSH) (Table 2.2) reported an average CO_2 concentration of 250-350 ppm as normal outdoor ambient air; 350 to 1,000 ppm as acceptable air quality; 1,000 to 2,000 ppm as poor air quality, and 2,000 to 5,000 ppm as harzard environment.

Table 2.2 Chronic exposure to elevated indoor CO_2 concentrations [10]

Concentration	Symptom
250 to 350 ppm	Normal background concentration in an ambient air
350 to 1,000 ppm	Concentrations in typical indoor spaces with good air ventilation
1,000 to 2,000 ppm	Drowsiness and poor air quality
2,000 to 5,000 ppm	Headaches, sleepiness, and stagnant, stale, followed by heart rate increase and nauseous feeling
5,000 ppm	Workplace exposure limit (as 8-hour TWA), regulated by most authority
> 40,000 ppm	Lead to serious oxygen deprivation that may cause permanent brain damage, coma and death

2.1.2 Elimination of CO_2

A well-known approach for industrial CO_2 capture is amine scrubber, in which amine compounds react with the CO_2 gas in presence of water to generate carbamates, and carbonic acid. Different types of amine include

- Monoethanolamine
- Diethanolamine
- Methyldiethanolamine
- Diglycolamine.
- The amine solution normally contains primary amine group ($-NH_2$) that undergoes acid-base reaction with CO_2, generating carbamates (Equation 2.1), and secondary amine (-NH) and tertiary amine (-N-) that endures CO_2 dissolution and amine catalyzed hydration [11]. He scrubbing tower normally was designed by spraying amine solution down from the top of the tower, flowing counter currently to the CO_2 stream coming from bottom to the top shown in Figure 2.1 [12]. The reaction is known to be an exothermic, and is reversed by temperature increase.

$$CO_2 + 2HOCH_2CH_2NH_2 \leftrightarrow HOCH_2CH_2NH_3^+ + HOCH_2CH_2NH\,(CO_2^-) \quad \text{Equation 2.1}$$

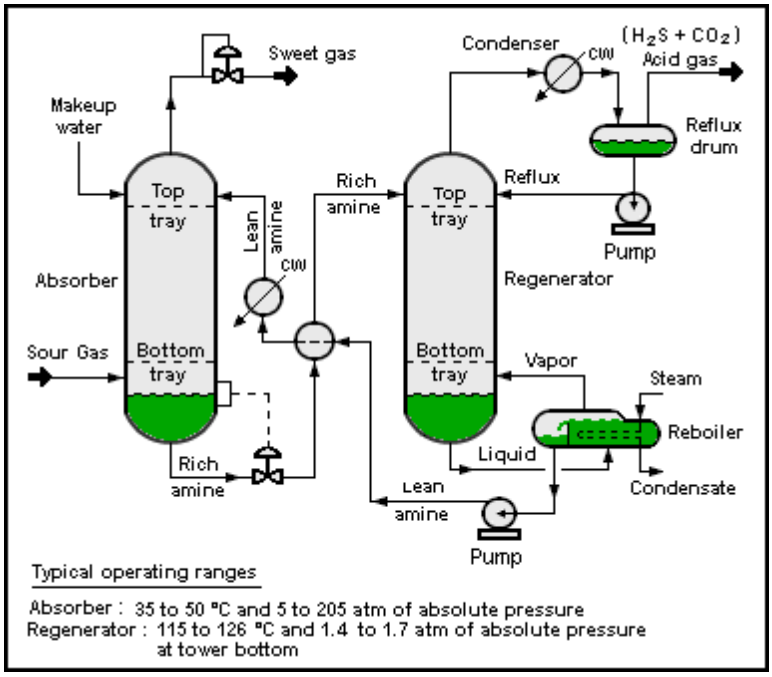

Figure 2.1 Process of scrubber CO_2 and H_2S [12]

2.1.3 Applications of CO_2

The CO_2 can be converted to dry ice, syngas, organic compound, generate electrical in power plant and combustion gas. Many researchers have demonstrated catalytic conversion of CO_2 to liquid/gas fuel, such as methane and methanol. A great deal of attention has turned to catalytic conversions of CO_2 and water to other energy source, getting rid of CO_2 and obtaining valuable products. In 2014, Li K. [4] and his team suggested that CO_2 can possibly be converted to methane, methanol and ethanol, relying on photocatalytic reaction. Although there have been reports on gas phase CO_2 conversion to Carbon monoxide, Hydrogen, Methane and methanol, an issue regarding the gas phase CO_2 conversion concerns its requirement on gas-tight system, and low energy content of the products. The photocatalytic conversion of CO_2 on TiO_2, an ultraviolet light activated catalyst, reforms CO_2 molecules to hydrocarbon substances, such as methane, methanol and ethanol. Groups of research enhanced TiO_2 catalytic activity by making it to TiO_2 nanoparticles, increasing surface to volume ratio of the particles, reducing their band gap energy. However, the nanoparticles, would suffer from particle agglomeration and lead to significant decrease in catalytic activity.

2.2 Photocatalyst

2.2.1 Background on photocatalyst

The photocatalyst is a material that needs UV and visible light activation to provide catalytic activity. Many metal oxides were demonstrated to be photocatalysts, such as titanium dioxide (TiO_2), zinc oxide (ZnO), and copper (II) oxide (CuO), etc, and were used as sensitive material in sensor devices, as electrodes in fuel cells, and in decomposing toxic organic compounds. In order to synthesize a good photocatalyst, material needs to be in nanoscale (nanoparticles), be in proper morphology (crystallography), and provide suitable energy band gap. When a photocatalyst is a introduced to photons from light, free electron (e^-) and hole (h^+) can

be created, leading to charge transfer cycles that activates electrons from valence band to conductive band [11] (Figure. 2.2).

$$O_2 + e^- \longrightarrow O_2^- \qquad \text{Equation 2.2}$$

$$H_2O + h^+ \longrightarrow OH + H^+ \qquad \text{Equation 2.3}$$

$$O_2 + e^- + H_2O + h^+ \longrightarrow O_2^- + OH^- + H^+ \qquad \text{Equation 2.4}$$

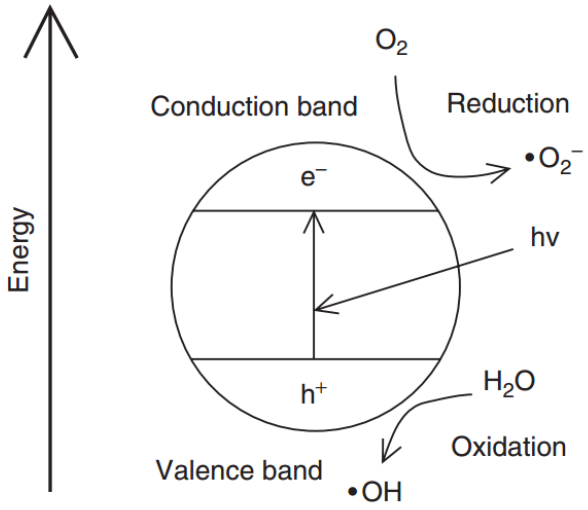

Figure 2.2 Reaction mechanism of a photo-catalyst [11]

Liu Y. and his team [13] used Bismuth Vanadate ($BiVO_4$) with photocatalytic activities to catalytically reform dissolved CO_2 to ethanol. It was concluded that yield of ethanol production can depend strongly on methods of catalyst synthesis, types of material, light source (wavelength and intensity), and wt.% loading of metal oxide on substrate.

2.2.2 Photoreaction of CO_2 covert to ethanol

Reaction mechanisms for CO_2 conversion to ethanol over metal oxide graphene catalyst are not well understood; however, Chang X. et.al [14] suggested the reaction mechanism as shown in equation 2.5 to 2.8. Chang [14] believed that water was photocatalytically dissociated to oxygen and proton, releasing 1 electron per water molecule. The electron from water yields electron activation on metal oxide

catalyst, jumping from valence band to conductive band. The active electron on the conductive band can interact with CO_2, generating carbon dioxide radicals (CO_2^-) that can further catalytically transformed to ethanol and water.

$$H_2O \longrightarrow H^+ + O_2 + e^-(\text{valance band}) \qquad \text{Equation 2.5}$$

$$e^-(\text{valance band}) \longrightarrow e^- (\text{conduction band}) \qquad \text{Equation 2.6}$$

$$CO_2 + 2e^-(\text{conduction band}) \longrightarrow \bullet CO_2^- \qquad \text{Equation 2.7}$$

$$2\bullet CO_2^- + 12H^+ + 8e^-(\text{conduction band}) \longrightarrow C_2H_5OH + 3H_2O \qquad \text{Equation 2.8}$$

The overall photocatalytic conversion of CO_2 to ethanol is concluded in equation 2.9.

$$2CO_2 + 12H^+ + 12e^- \longrightarrow C_2H_5OH + 3H_2O \qquad \text{Equation 2.9}$$

2.2.3 Energy band gap

Energy band gap is energy difference of an electron in valence band and conduction band (Figure 2.3) A huge energy gap is present in an insulating material while the conduction and the valence bands overlap in case of conducting material. A semiconductor is somewhere in the middle where the conductive and the valence bands are narrowly separated. Electrons in a semiconductor can be activated via UV radiation, light or other free electrons, presence of impurity (doping), and temperature, etc. [15].

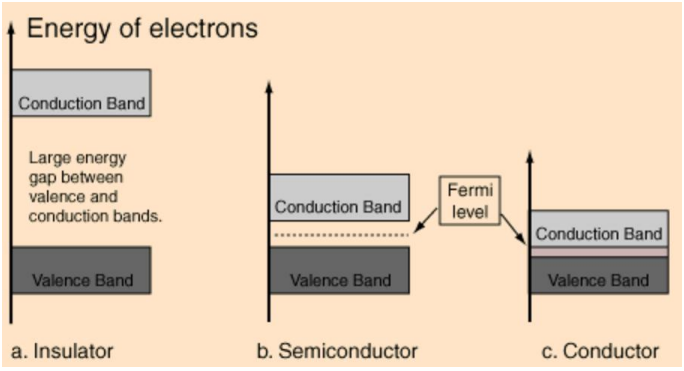

Figure 2.3 Energy band gap of a) insulator, b) semiconductor and c) conductor [15]

In other words, band gap energy is a minimum amount of energy required to activate electron from valence to conductive band. Basic method for a determination of band gap value depend on “Tauc plot” that follows correlation of UV light absorbance and band gap energy (equation 2.10) [16].

$$\alpha hf \quad \alpha \quad (hf - E_g)^n \qquad \text{Equation 2.10}$$

where "hf" is the photon energy, E_g is the band gap energy, and $n = 2$ for indirect transition, $n = ½$ for direct transition phenomena.

$$\alpha = 1/dA \qquad \text{Equation 2.11}$$

Where d is the thickness of quartz cell and A is the absorbance value. Zhang D. and her team [17] used Tauc equation for an energy band gap determination of TiO_2, GO and TiO_2/GO. The energy band gap was obtained from an extrapolation of linear regression region of $(\alpha hf)^{1/2}$ vs hf plot (Figure. 2.4).

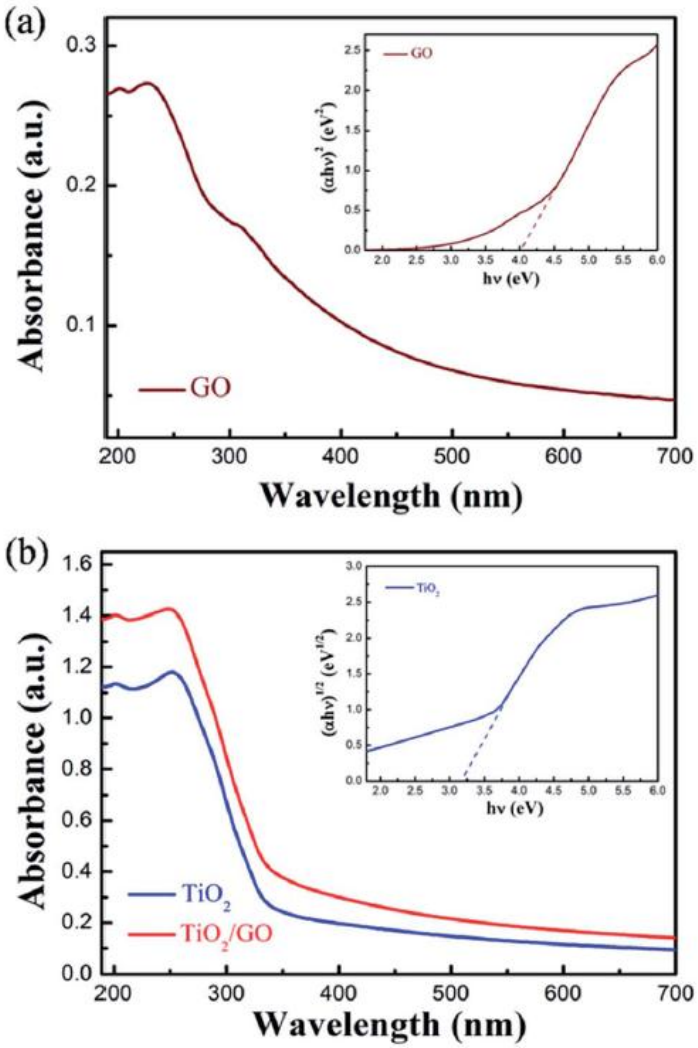

Figure 2.4 UV-visible spectra of (a) GO and (b) TiO_2 film and TiO_2/GO hybrid film[17].

2.3 Titanium dioxide graphene composite (TiO_2/rGO)

2.3.1 Titanium dioxide (TiO_2)

Titanium dioxide is a metal oxide that is widely used as a photocatalyst. TiO_2 can be activated by the UV light (>390nm.), pushing electrons from valence to conduction band, generating holes (h^+) and free electrons. Crystallography of TiO_2 include anatase, rutile and brookite phase (Figure. 2.5).

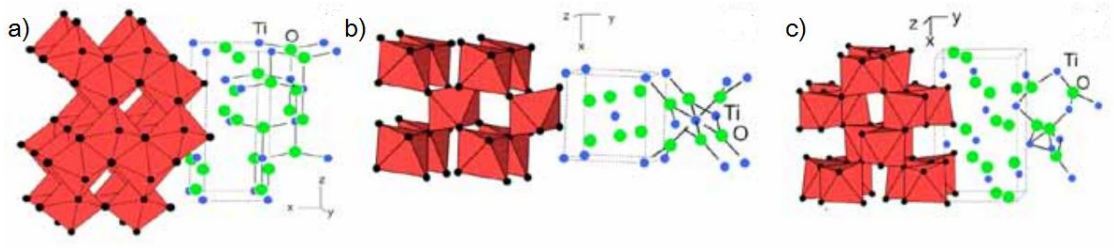

Figure 2.5 Crystallographic structures a) anatase b) rutile and c) brookite phase of TiO_2 [18]

Temperature and pressure change can trigger phase transformation in TiO_2 (Figure. 2.6), providing different molecular structures that lead to different chemical and physical properties.

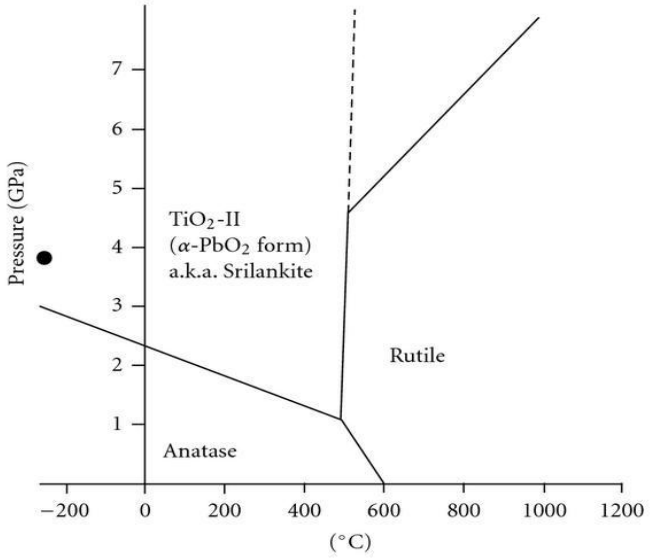

Figure 2.6 Phase diagram of TiO_2[18]

At ambient conditions, anatase and rutile are two dominant phases of TiO_2, in which anatase is more photocatalytically active and provides higher surface area. On the other hand, rutile phase presents lower band gap energy (Table 2.3), offering better catalytic performance as compared to anatase [18]. Combination of anatase and rutile phase on TiO_2 has been demonstrated to perform well as photocatalyst at ambient conditions

Table 2.3 Physical property of anatase and rutile[18]

Physical properties	Rutile	Anatase
Structure	Orthorhombic	Orthorhombic
Energy band gab (eV)	3.030	3.200
Hardness(Mohs)	6.0-7.0	5.5-6.0
Density (g/cm^3)	4.250	3.894
Gibbs free energy (kcal/mol)	-212.6	211.4
Melting point (C°)	1858	Changing phase at 600

Various methods have been proposed for a synthesis of TiO_2 nanoparticles. Go´rska and his team used sol-gel method [19] for TiO_2 synthesis, starting by hydrolyzing titanium (IV) isopropoxide in distilled water. The suspension was stirred at 80^oC for 12 hours before the precipitate was filtratetd, rinsed with ethanol, dried at 80^oC for 12 hours, and calcinated at 350 to 750 ^oC for 2 hours. The photocatalytic activity of TiO_2 was tested by decomposing phenol under visible and ultraviolet light. It was found that the TiO_2 (450^oC calcination temperature) provided the best catalytic activity under UV light [19], as resulted from low energy band gap and high surface area of the material (Table 2.4 and Figure. 2.7).

Table 2.4 Characteristics of the TiO_2 catalysts, calcinated at different temperatures [19]

Physical property	350^oC	450^oC	550^oC	650^oC	750^oC
Band gap energy(eV)	3.41	3.33	3.31	3.27	3.04
BET surface area(m^2/g)	205.8	180.2	147.7	93.5	8.3
Pore volume(cc/g)	0.43	0.43	0.4	0.26	0.03
Average crystallite size(nm)	8.4	10.2	10.9	28.4	58.6

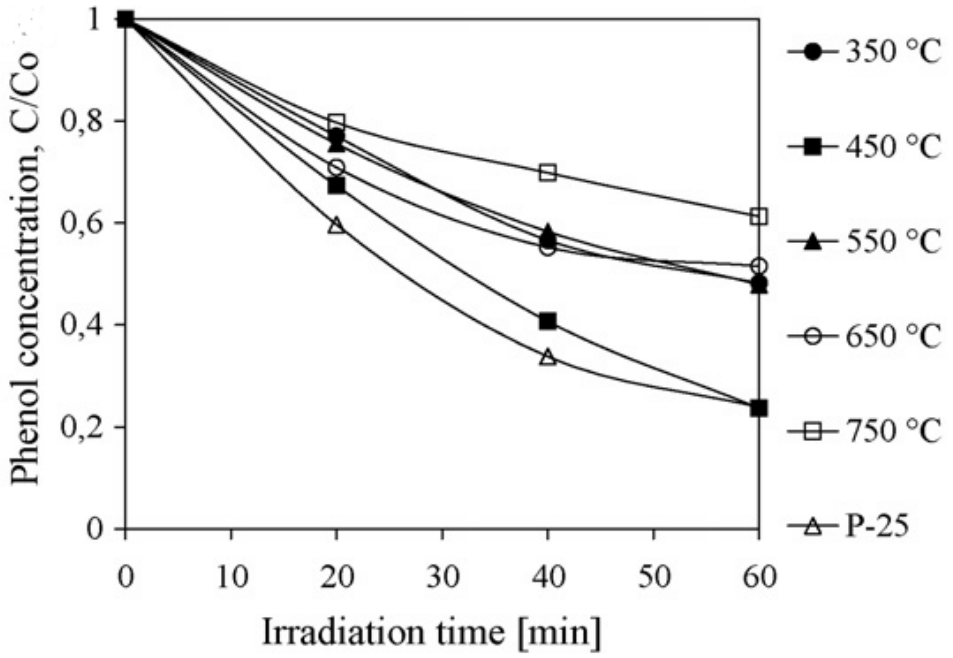

Figure 2.7 Degradation of phenol using TiO2 photocatalysts at varying calcinating temperature under visible light. [19]

There were research works on photoreaction process. For example, Rajalakshmi K. and his team studied characteristics and performances of the two commercial grade TiO_2 photocatalyst, P25 and Hombikat UV-100, with those o the sol-gel TiO_2. The TiO_2 assisted photocatalytic conversion of CO_2 under alkaline solution and UV-visible light (400-600 nm) alteration. Methane, methanol and ethanol were observed, as shown in table 2.5 [20].

Table 2.5 Yields of production [20].

Catalyst	Methane(µmol/g)	Methanol(µmol/g)	Ethanol(µmol/g)
P25	0.7	914	0
Hombikat UV-100	0.3	118	53
Sol-gel	0.6	130	59

Reaction mechanisms started with activation of TiO_2 with UV-visible light, followed by water dissociation and equilibrium of protons hydroxyl and oxygen (equation 2.12 to 2.17).

$$TiO_2 + hf \longrightarrow e^- + h^+ \quad \text{Equation 2.12}$$

$$H_2O \longrightarrow H^+ + OH^- \quad \text{Equation 2.13}$$

$$H^+ + e^- \longrightarrow H\bullet \quad \text{Equation 2.14}$$

$$OH^- + h^+ \longrightarrow OH\bullet \quad \text{Equation 2.15}$$

$$2OH\bullet \longrightarrow H_2O_2 + h^+ \longrightarrow O_2^- + 2H^+ \quad \text{Equation 2.16}$$

$$O_2^- + h^+ \longrightarrow O_2 \quad \text{Equation 2.17}$$

The CO_2 conversion involves CO_2 dissolution, transfer of electrons, protons, and radicals (equation 2.18 to 2.25). Reaction mechanisms were identified by Electron Spin Resonance Spectroscopy (ESR), indicating elemental analysis of C, H, CH_3 radicals and Ti ions on TiO_2 in presence of CO_2 and water at 77 K.

$$CO_2 + e^- \longrightarrow \bullet CO_2^- \quad \text{Equation 2.18}$$

$$\bullet CO_2^- + H\bullet \longrightarrow CO + OH^- \quad \text{Equation 2.19}$$

$$CO + e^- \longrightarrow \bullet CO^- \quad \text{Equation 2.20}$$

$$\bullet CO^- + H\bullet \longrightarrow \bullet C + OH^- \quad \text{Equation 2.21}$$

$$\bullet C + H^+ + e^- \longrightarrow \bullet CH \longrightarrow \bullet CH_2 \longrightarrow \bullet CH_3 \quad \text{Equation 2.22}$$

$$\bullet CH_3 + H^+ + e^- \longrightarrow CH_4 \quad \text{Equation 2.23}$$

$$\bullet CH_3 + OH^- \longrightarrow CH_3OH \quad \text{Equation 2.24}$$

$$\bullet CH_3 + \bullet CH_2 + e^- \longrightarrow C_2H_5OH \quad \text{Equation 2.25}$$

On the other hand, Rajalakshmi K. [20] suggested reaction mechanisms for Photocatalytic conversion of CO_2 using IR spectroscopies, shownin Figure. 2.8.

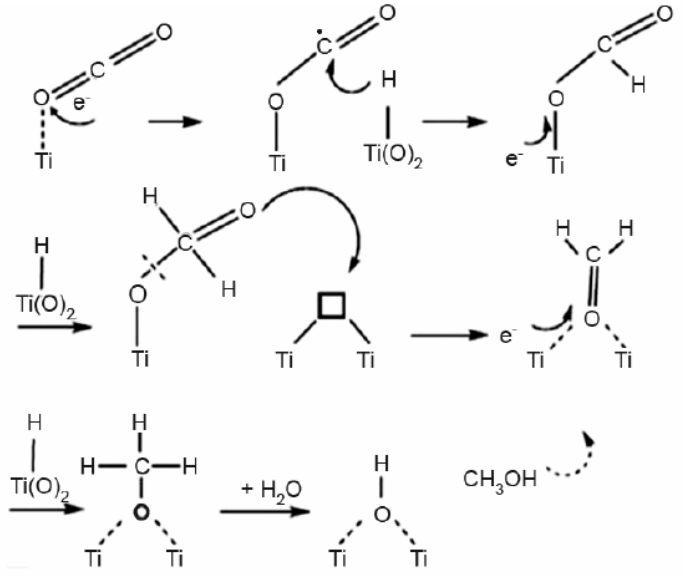

Figure 2.8 Reaction partway for photocatalytic reduction of CO_2 by water on TiO_2 [20]

Photoreaction of CO_2 to methane, methanol, and ethanol was explaned by a reaction of $\bullet CH_3$ radical with $\bullet OH$, $\bullet H$ or $\bullet CH_3$, generating methanol, ethane, and methanol, respectively (Figure 2.9).

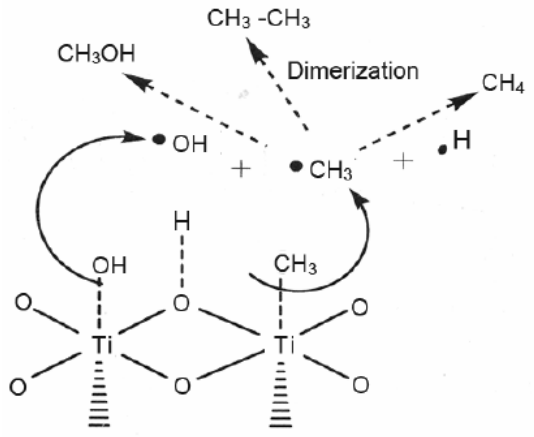

Figure 2.9 Mechanisms for methanol production, assisted by TiO_2(Rajalakshmi K.) [20].

The $\bullet CH_3$ radical can further react with $\bullet CH_2$ to become CH_3-$CH_2\bullet$ that combine with $\bullet OH$ to become ethanol (Figure 2.10).

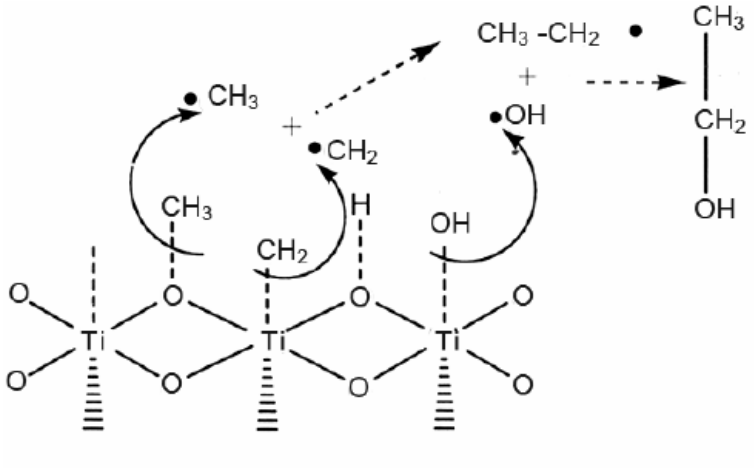

Figure 2.10 Mechanisms for ethanol production, assisted by TiO_2 catalyst [20]

For methane production, $\bullet CH_3$ radical reacted with $\bullet OCH_3$, forming ether, and eventually methane and formaldehyde (Figure 2.11).

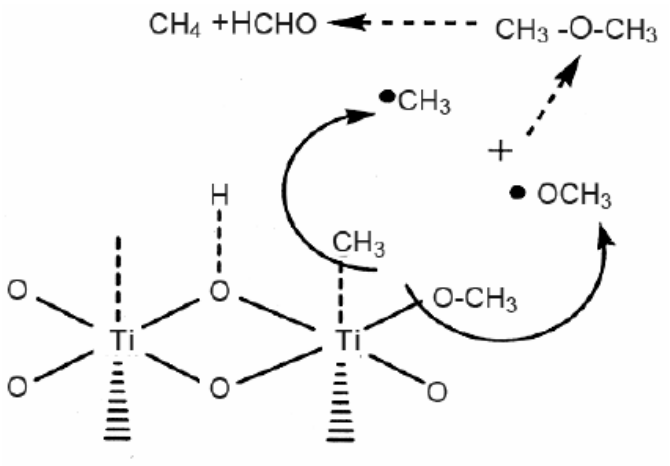

Figure 2.11 Mechanisms for methane generation, assisted by TiO_2 catalyst. [20]

Oluwafunmilola O. and his team [14,21] reported a photoreaction of CO_2 with helps from TiO_2 catalyst, shown in equation 2.26-2.28.

$$CO_2 + 8H^+ + 8e^- \longrightarrow CH_4 + 2H_2O \qquad \text{Equation 2.26}$$

$$CO_2 + 6H^+ + 6e^- \longrightarrow CH_3OH + H_2O \qquad \text{Equation 2.27}$$

$$2CO_2 + 12H^+ + 12e^- \longrightarrow C_2H_5OH + 3H_2O \quad \text{Equation 2.28}$$

Moreover, there were reports on plasmonic effect of silver nanoparticle that can enhance photocatalytic activity, based on their surface plasmon resonance (SPR) effect. The effect provides free electron's oscillation at metallic surface, induced by visible light irradiation in an appropriate range. Liu E. team [22] and Kocˇi K. team [23] found benefits in doping silver nanoparticle at various wt. % on TiO_2, and explained the reaction mechanisms as followed.

$$TiO_2 + hf \longrightarrow h_{vb}^+ + e_{cb}^- \quad \text{Equation 2.29}$$

$$e_{cb}^- \longrightarrow e_{Ag}^- \quad \text{Equation 2.30}$$

$$e_{Ag}^- + hf\ (\text{visible light}) \longrightarrow e_{SPR}^- \quad \text{Equation 2.31}$$

$$h_{vb}^+ + H_2O \longrightarrow H^+ + OH^- \quad \text{Equation 2.32}$$

$$CO_2 + 6e_{SPR}^- + 4H^+ \longrightarrow CH_3OH \quad \text{Equation 2.33}$$

Where hf is the photon energy, $h_{vb}^+$is the hole at valance band, $e_{cb}^-$is the free electron at conduction band, $e_{Ag}^-$is the free electron at silver nanoparticle and e_{SPR} isthe free electron from SPR effect.

Although it was claimed in the paper that visible light helped increasing catalytic performance of the Ag-TiO_2 system, not much methanol was produced and detected (Figure 2.12 and 2.13 [22,23]).

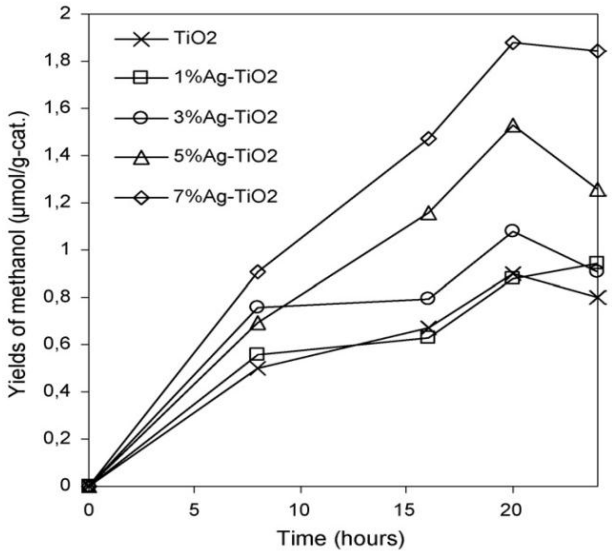

Figure 2.12 Reliance on reaction time of methanol production using the Ag-modified TiO_2 catalyst [22].

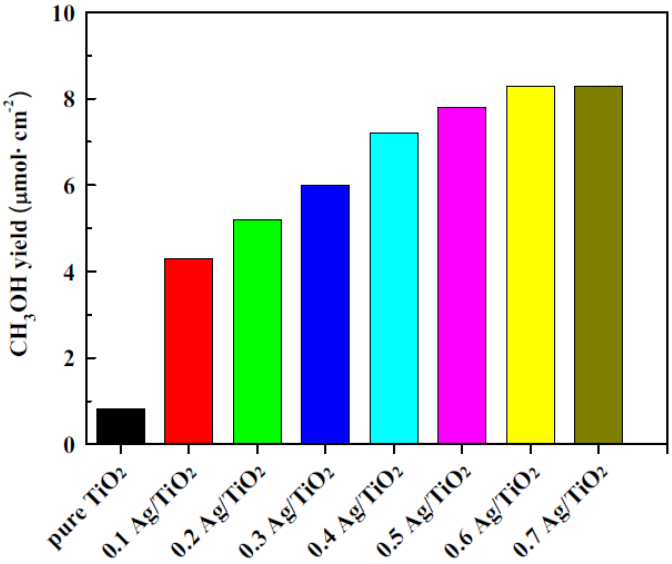

Figure 2.13 Methanol yields from a photoreduction of CO_2[23].

Slamet and his team [5] studied photocatalytic reaction of CO_2 in alkaline solution at liquid/solid interface of copper-doped titanium dioxide catalyst. Their results suggested that the photocatalysts with an oxidation number 2+ (Cu^{2+}) and copper with 3%wt loading yielded highest amount of methanol as shown in Figure 2.14.

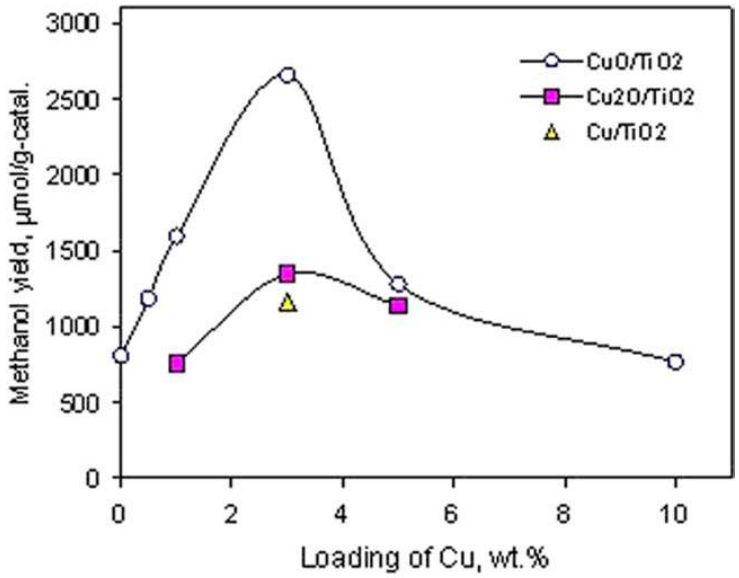

Figure 2.14 Effect of copper loading amount of methanol [5]

It was evident by E^0 energy that cupric ions (Cu^{2+}) prefer accepting one electron to 2 electrons, and that one step reduction process (Equation 2.34) required less amount of energy as compared to two steps process (Equation 2.35 and Equation 2.36).

$$Cu^{2+} + 2e^- \longrightarrow Cu^0 \qquad E^0 = 0.34\ V \qquad \text{Equation 2.34}$$

$$Cu^{2+} + e^- \longrightarrow Cu^+ \qquad E^0 = 0.17\ V \qquad \text{Equation 2.35}$$

$$Cu^+ + e^- \longrightarrow Cu^0 \qquad E^0 = 0.52\ V \qquad \text{Equation 2.36}$$

Also, Cu^{2+} (CuO) is effective in obtaining 1 electron (Equation 2.34) and becomes Cu^+. The reduction of cupric (Cu^{2+}) to cuprous (Cu^+) ions can be reversed via Cu^+ donating 1 electron to proton. The whole process was presented in Equation 2.37.

$$CuO \xrightarrow{e^-} Cu_2O \xrightarrow{O_2/H^+} CuO \qquad \text{Equation 2.37}$$

2.3.2 Graphene

Graphene is an allotrope of carbon with 2-dimensional nanostructures (Figure 2.15). Its outstanding electrical/chemical/mechanical properties secure its place as an advanced material for a wide spectrum of applications. For example, graphene is ~100 times stronger than steel, has a hypothetical thickness of 3.35Å, provides excellent heat and electrical charge conduction. Researchers worldwide has paid great interests in utilizing graphene and its composites for various applications; electronic components, electronic devices, and catalyst supports, etc.

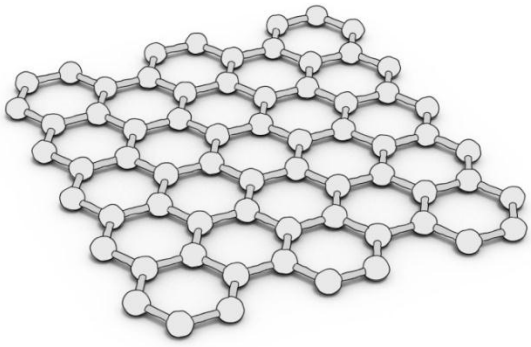

Figure 2.15 Schematic diagram of graphene structure

Several methods were proposed and demonstrated for graphene synthesis, such as chemical vapor deposition (CVD), mechanical exfoliation, and chemical exfoliation. The Chemical vapor deposition method used carbon sources that underwent catalytic decomposition over catalyst (Copper and Nickel, in general), and became graphene sheets. Although a close-to-perfect graphene structure could be obtained, high investment cost for operation apparatus and low production yields were two main issues for the CVD method. The mechanical approach relied on physical contact of glued tape and highly crystalline graphite, leading to mechanical separation of graphene sheets from the bulk graphite. Major drawbacks from mechanical exfoliation method concerned permanent glue islands that were adhered on the graphene sheets, relatively small graphene piece, and low yields. Then, the chemical exfoliation could be an appropriate method for good quality, and gram-scale production of graphene. The method utilized chemical oxidation of graphite with strong oxidizing agent in acidic solution. The reactions indulge functional groups, such as hydroxyl, carbonyl and carboxylic, on graphite structures. The functional

groups could provide electrostatic charges on each graphite layers, resulting in isolation of layers, becoming graphene sheets (Figure 2.16).

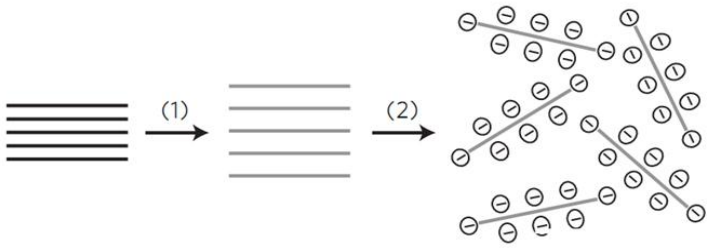

Figure 2.16 Synthesize graphene oxide; (1) Oxidation of graphite using oxidizing agent in strong acid solution; (2) Isolation of graphite layers to graphene oxide sheets[1].

Most chemical exfoliation methods were modified from Hummers' method, introduced by Hummers S.W. and his groups in 1958 [8] Hummers demonstrated synthesis of "graphitic oxide", later known as graphene oxide (GO), using chemical oxidation of graphite and potassium permanganate in concentrated sulfuric acid solution [8]. The GO, with C-O-H functional groups, was electrically insulating and was not suitable for electronic applications. If needed, GO can be chemically reduced with reducing agent, i.e. L-ascorbic acid, or underwent thermal reduction, to become a semiconductive reduced graphene oxide (rGO) (Figure 2.17).

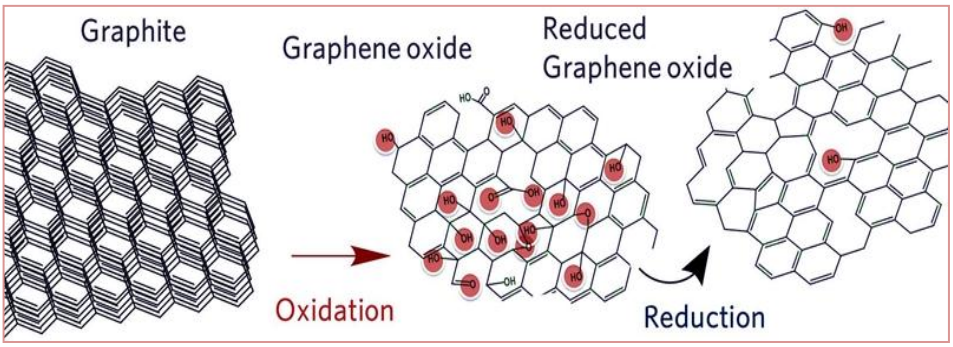

Figure 2.17 Different oxidative states of graphene[2]

[1] http://pubs.rsc.org/services/images/RSCpubs.ePlatform.Service.FreeContent.ImageService.svc/ImageService/Articleimage/2012/RA/c2ra00663d/c2ra00663d-f1.gif

[2] http://materialschemistry.utu.fi/wp-content/uploads/2015/12/GO-to-rGO.jpg

Graphene oxide (GO) with functional groups can serve as a supporting material for metal/metal oxide catalyst. Electrostatic charge on GO could attract and accumulate cations from liquid solution, acting as preferred nodes for metal/metal oxide deposition/precipitation. Composite material of TiO_2/rGO can be chemically synthesized, following standard sol-gel method, providing TiO_2 as photocatalyst, immobilized on GO sheet. Li X. and his teams [24, 25] had published works on synthesis and performance of copper oxide (Cu_2O)-graphene composite (Cu_2O/GO) in photocatalyzing CO_2 to methanol in water medium. Their results showed catalytic activity of the composite in producing methanol (Figure 2.18). Later on, Li and his groups demonstrated that ZnO-graphene composite also had ability in converting CO_2 to methanol (Figure 2.19) [25].

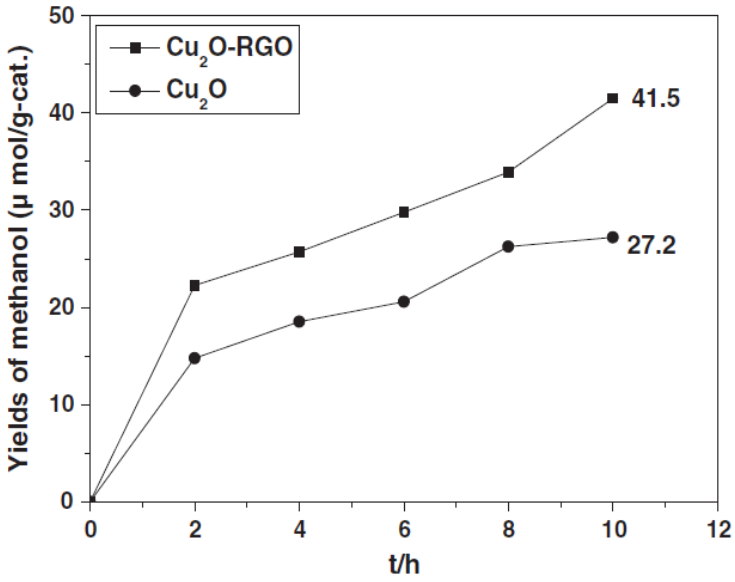

Figure 2.18 Methanol yields from Cu_2O and Cu_2O-rGO at various operating time [24]

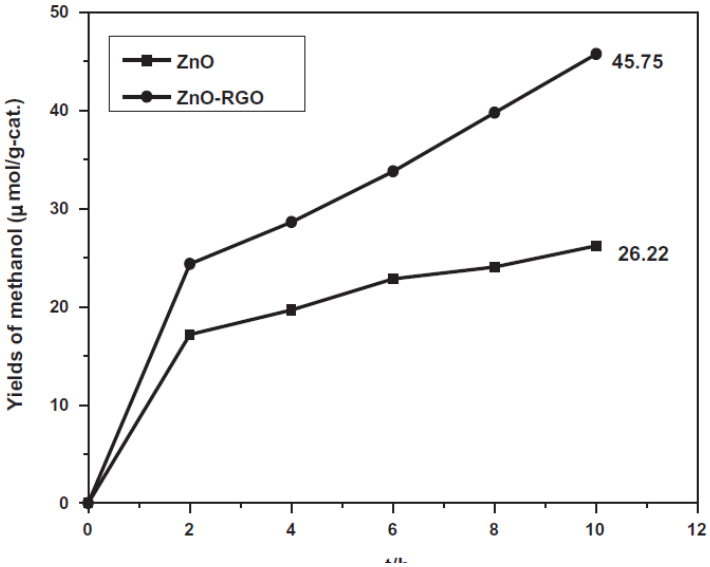

Figure 2.19 Methanol yields from ZnO and ZnO-rGO at various operating time [25]

Zhang Q. and his team [26] studied photocatalytic reaction of CO_2 in alkaline solution at liquid/solid interface of TiO_2/rGO catalyst. TiO_2/rGO was synthesized by hydrothermal method using commercial-grade TiO_2. It was observed that the TiO_2 only has an affinity for UV-light adsorption; but, with an addition of Graphene, the TiO_2/graphene composite extent light adsorption range of the composite to visible light (Figure 2.20). Then, one great advantage of a TiO_2/graphene composite is the enchanced light adsorption ability that helps promoting photocatalytic activity of the catalyst.

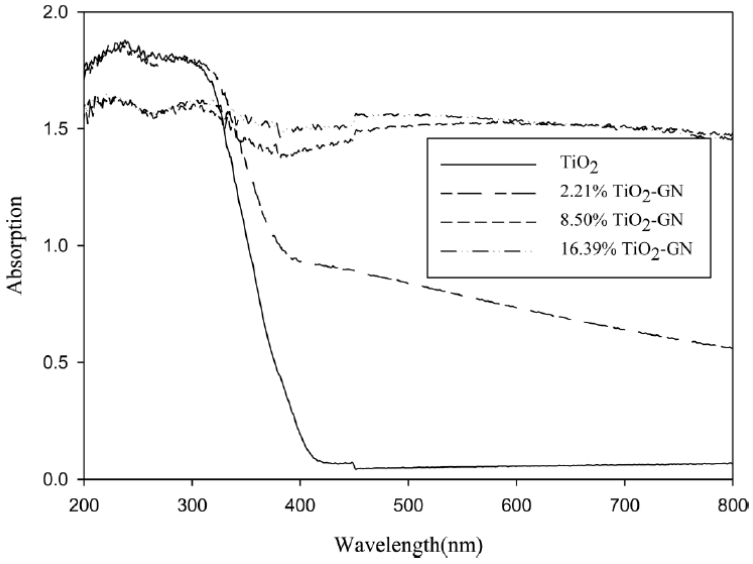

Figure 2.20 UV-Vis absorption spectra of TiO_2 and TiO_2/rGO catalysts

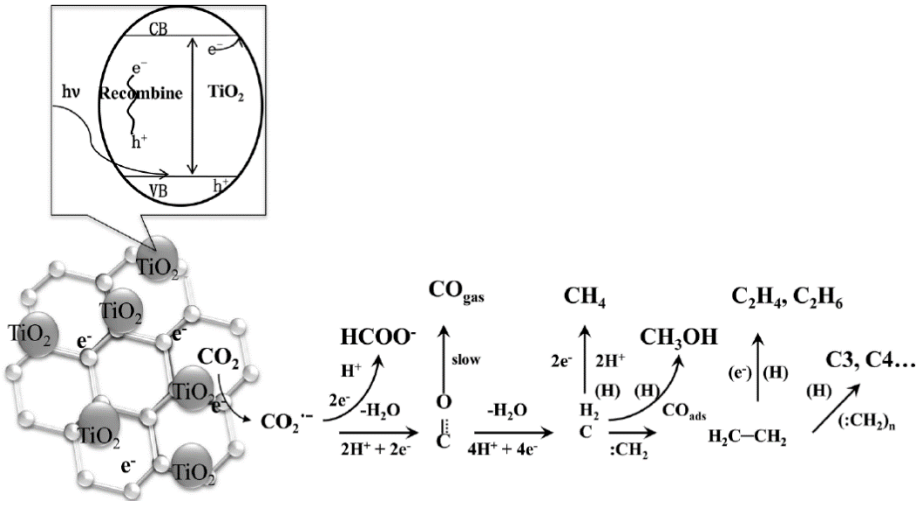

at different TiO_2 loading on rGO [26]

Figure 2.21 The mechanism of carbon dioxide reduction [26]

Mechanism of photocatalytic reaction of CO_2 in liquid phase is shown in Figure 2.21. The TiO_2 catalyst is activated by the photons, urging electrons to jump up from valence band to conductive band. It was noted that graphene helps reducing recombination rate of electrons and holes in the TiO_2/rGO composite, and promoting the amount of active electrons in the material. The CO_2 accepts one active electron from TiO_2 and undergoes various reaction paths with water and proton. The CO^{2-}

radical can couple with proton to form $HCOO^-$ radical, that can further emit CO gas and become carbonyl (C=O) based substances. Combination of carbonyl and water leads to either a generation of methane or methanol, which can be acquired as energy source. However, series of catalytic reactions can continue and produce bigger hydrocarbon molecules, such as ethane, ethane, butane, etc. Since protons involve heavily in the reactions, solution pH is a vital effect for CO_2 photocatalytic conversion. However, although protons are needed in the reactions, too many protons lower solution pH and adverse CO_2 dissolution, reducing precursors, e.g. bicarbonate, and decreasing rate of the reactions [26]. In this case, the highest methanol yield was achieved at pH value of 5.

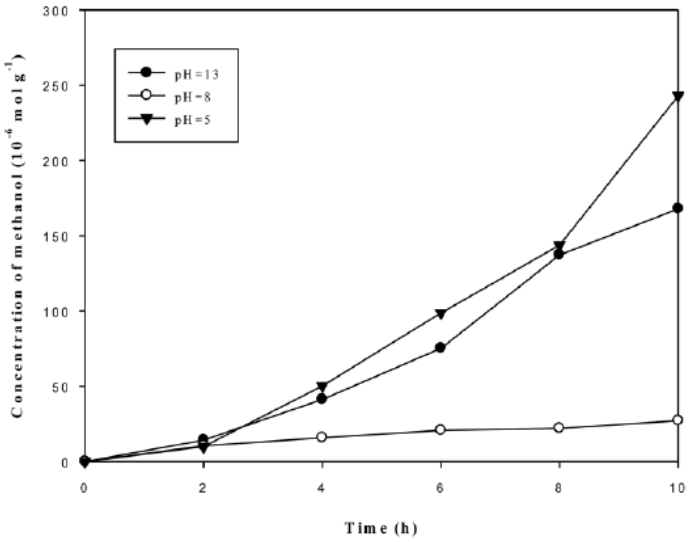

Figure 2.22 CO_2 photocatalyzed reduction at different pH values [26]

Although 16.39% TiO_2/rGO has the highest specific surface area (Table 2.6), but 2.21% and 8.54% TiO_2/rGO, both having much lower surface area, achieved higher methanol production yield than 16.39% TiO_2/rGO as shown in Figure 2.23. This could be attributed to other factors, which require further investigation.

Table 2.6 Comparison of specific surface area, total pore volume, and average pore width of TiO_2-GN samples [26]

Sample	Specific surface area (m^2 g^{-1})	Total pore volume (cm^3 g^{-1})	Average pore width (nm)
2.21% TiO_2-GN	64.92	0.38	23.74
8.50% TiO_2-GN	101.05	0.29	11.53
16.39% TiO_2-GN	115.84	0.24	8.29

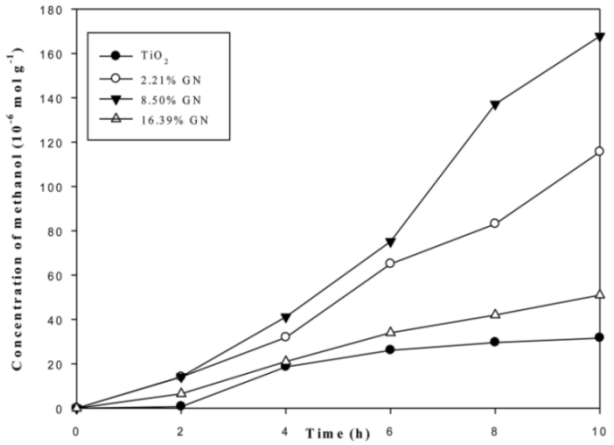

Figure 2.23 Photocatalytic reduction of carbon dioxide by the various catalysts. [26]

From Figure 2.21, photo-reaction of CO_2 in water can also yield H_2, CO, and CH_4 as side products. Liu J. and his team [27] studied photocatalytic reaction of CO_2 in gas and liquid phase. TiO_2/rGO composite was synthesized at the weight ratio between TiO_2 and graphene was varied at 1:1 and 10:1. The quantity of methanol and CH_4 produced with the photo-reaction were measured every hour. Only methanol was observed when using pure TiO_2, while TiO_2/rGO can yield both methanol and methane as shown in Figure 2.24.

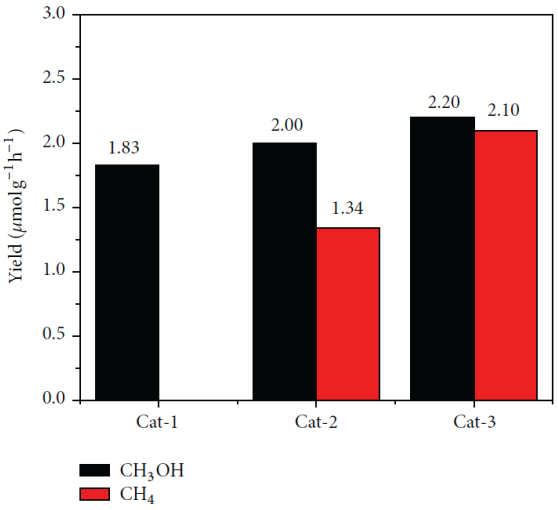

Figure 2.24 Comparison of photocatalytic activity of samples Cat-1 (TiO_2 pure), Cat-2 (TiO_2/rGO composite at ratio 1:1), and Cat-3. (TiO_2/rGO composite at ratio 10:1) [27]

CHAPTER III
MATERIALS AND METHODS

3.1 Synthesis of graphene oxide

The GO powder was chemically synthesized using a modified Hummers method [8]. In a general, graphite flakes (Alfa Aesar, 99.9%, 10 mesh, 2 grams) was mixed with sodium nitrate ($NaNO_3$, Fluka chemika, 99.0%, 1 gram) in a 250-ml flask, containing concentrated sulfuric acid (H_2SO_4, ACl Labscan, 98 %, 50 ml). The mixture was stirred continually in an ice-bath cooled container while potassium permanganate ($KMnO_4$, UNIVAR, 99.0%, 7.3 grams) was slowly added in during 2.5 hours period. Then, the mixture was warmed up to room temperature (~35°C), and stirred for another 2.5 hours. The mixture became viscous and was diluted using DI water (90 ml), followed by an addition of hydrogen peroxide (H_2O_2) solution 7 ml H_2O_2 (Mercks, 30%) and 55 ml DI water. Excess manganese radicals from potassium permanganate was converted to water-soluble MnO_2, and filtered out along with the filtrate using vacuum filtration apparatus and micro filter paper (GF/C, Whatman).The GO was obtained as brownish-color powder, and was further rinsed with 3%v/v of hydrochloric (HCl, ACl Labscan, 37%) and DI water, sequentially, using centrifuge, and dried in an oven at 90^{o}C for 12 hours. (Figure 3.1).

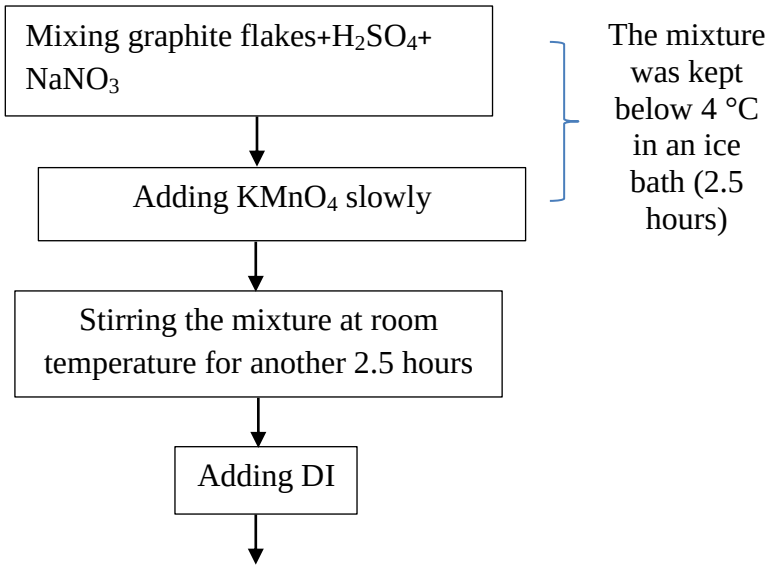

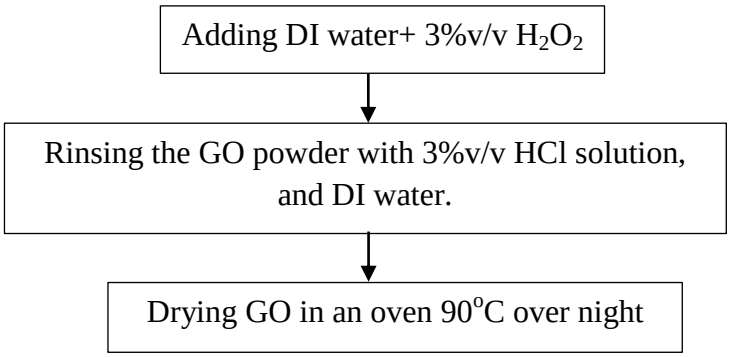

Figure 3.1 Flow chart of GO synthesis

3.2 Synthesis of TiO_2/rGO composite

The TiO_2/rGO composite was synthesized following sol-gel method that involved resuspension of GO in a 1:1 (10 ml: 10 ml) mixture of DI water and ethanol (0.1 grams GO/ml DI water). A solution of titanium (IV) butoxide ($Ti(OC_4H_9)_4$, Sigma-Aldrich, 97%) in ethanol was added to the GO solution(using ultrasonic). The amount of $Ti(OC_4H_9)_4$, used in the synthesis of TiO_2/GO, was determined by weight ratio of TiO_2:GO, assuming that all the $Ti(OC_4H_9)_4$ converted to TiO_2 and attached to graphene. The amount of $Ti(OC_4H_9)_4$ was varied from 10 to 20, 30, 40, 50, and 60 %wt, resulting in TiO_2/GO composite with different amount of TiO_2 loading. Then, the mixture was vaporized at 90°C for 2 hours, obtaining the TiO_2/GO composite powder that would further be calcinated in a furnace at 450°C for 2 hours (Figure 3.2). Noting that GO can undergo thermal reduction process, becoming reduced graphene oxide (rGO). The composite after calcination was, then, known as TiO_2/rGO.

While keeping the amount of $Ti(OC_4H_9)_4$ at 40%wt, effect from time of reaction was investigated by varying reaction time from 3 to 6, 12 and 24 hours, respectively, and observed changes in physical geometry under the transmission electron microscope (TEM).

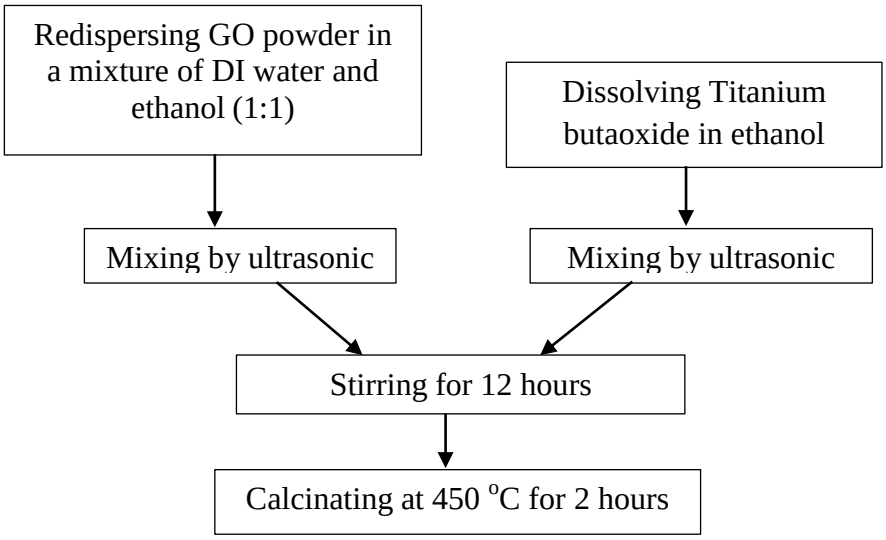

Figure 3.2 Flow chart of TiO_2/rGO synthesis

3.3 Synthesis of CuO-TiO_2/rGO composite

Copper(II)oxide was doped on TiO_2 at different %wt loading (0.3-2wt%) using sol-gel synthesis method. First, titanium solution was prepared by mixing $Ti(OC_4H_9)_4$ with ethanol. Copper solution was prepared by dissolving Copper(II)nitrite pentahydrate ($Cu(NO_3)_2{\cdot}5H_2O$) in DI water and ethanol (volume ratio of 1:1). Then, the copper solution was slowly added into the titanium solution, stirred for 3 hours and maintained at 25°C for 24 hours. It was further calcined at 450°C for 2 hours, forming firstly the CuO-TiO_2 particles. Graphene solution was prepared by re-dispersing reduced graphene oxide in DI water and ethanol (volume ratio of 1:1), mixed 50 mL with the CuO-TiO_2 particles, and stirred for 2 hours at room temperature. Finally, the mixture was stirred for 1 hour at 120°C, and dried at 90°C for 12 hours, yielding CuO-TiO_2/rGO composite. Noting that the CuO-TiO_2/rGO composite was synthesized following the maximum ethanol yield, obtained from 20%wt TiO_2 loading on the TiO_2/rGO composite. The Copper(II)oxide loading was varied from 0.5 to 2wt% while the TiO_2 loading was kept constant a t 20% loading

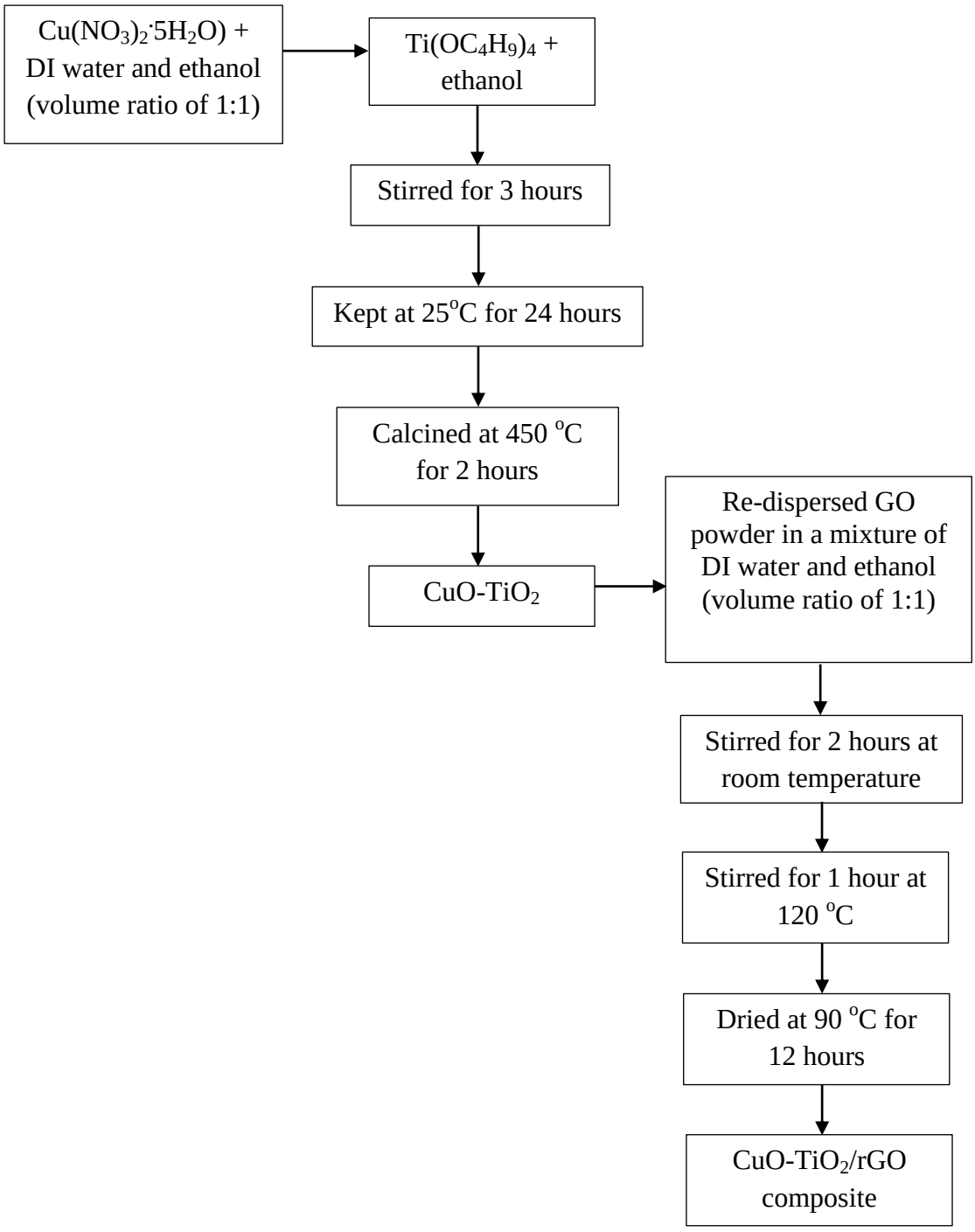

Figure 3.3 Flow chart of $CuO\text{-}TiO_2$/rGO Synthesis

3.4 Photocatalytic conversion of CO_2

In the Figure 3.4, the composite material was suspended in a stirred flask containing 100 ml DI water (1g composite/liter water). The mixture was then employed in an in-house made reaction chamber (at 45 ^{o}C). The chamber consisted of a mercury lamp bulb (Philip 160 W) located right above the flask that was continually stirred by magnetic stirrer. All components were concealed inside a light reflecting box. Before an operation, carbon dioxide gas (CO_2) would be bubbled through the mixture contained in the flask at a flow rate of 100 ml/min for 30 mins (in Figure 3.4). The CO_2 would undergo CO_2 dissolution generating carbonic acid that was necessary as a reactant for photocatalytic conversion of CO_2. The liquid solution from the reactor was sampled using syringe filter and kept in a sealed viol for characterizations. The samples were characterized for methanol composition using gas chromatography (7890A, Agilent Technologies) with EPA method 308.

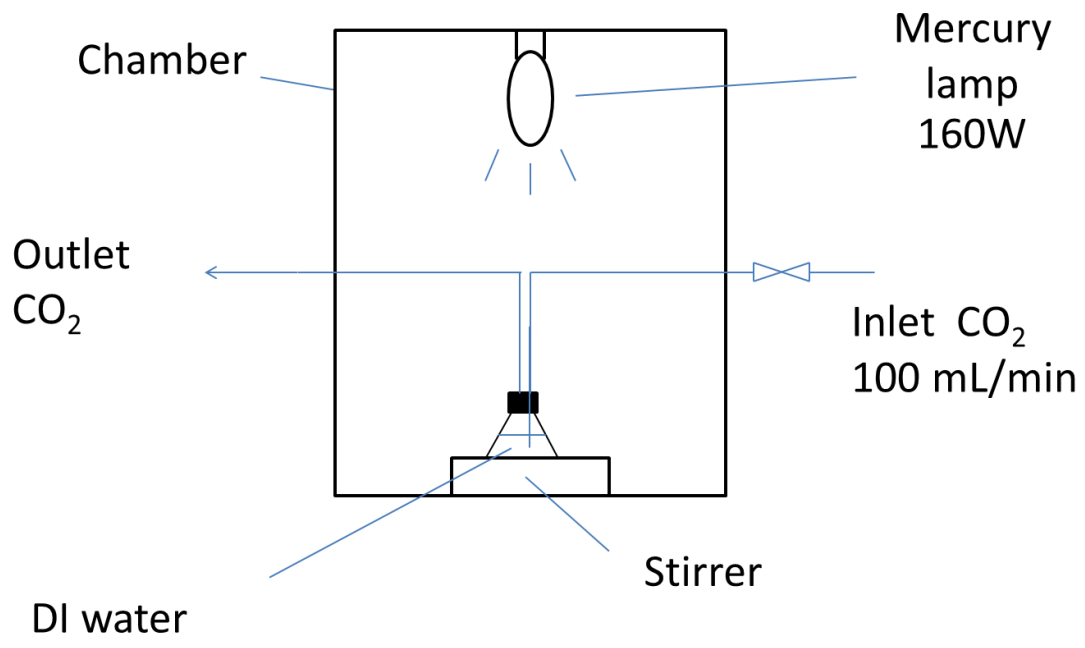

Figure 3.4 Schematic diagram of the photocatalyst reactor

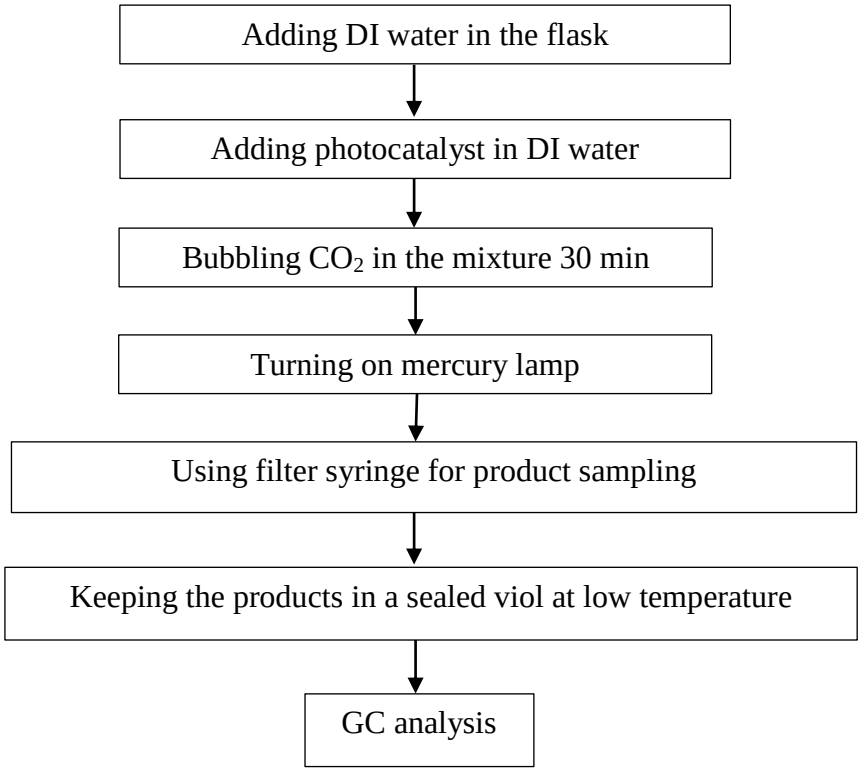

Figure 3.5 Photocatalyst reaction

CHAPTER IV
RESULTS AND DISCUSSION

4.1 TEM and SEM analysis

TEM image (Figure 4.1) shows the physical geometry of graphene and graphene composite. Figure 4.1(a) exhibits flat and transparent carbon sheet of graphene, while Figure 4.1(b) displays distribution of TiO_2 nanoparticles on graphene sheet, with equivalent diameter size of 8-10 nm.

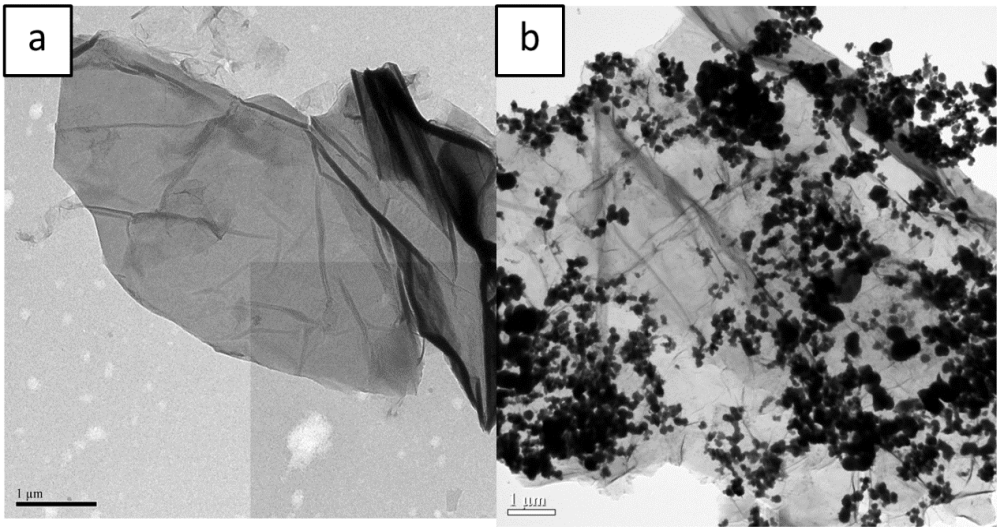

Figure 4.1 TEM images of a) Graphene oxide (GO). and b) TiO_2/rGO composite (40wt.% TiO_2 loading)

4.1.1 TiO_2/rGO

During the synthesis of TiO_2/rGO with sol-gel method, $Ti(OC_4H_9)_4$ participated in hydrolyzed reaction with water and ethanol resulting $Ti(OC_4H_9)_4$ covert to $Ti(OH)_4$, $Ti(OC_2H_5)_x(OC_4H_9)_y$, TiO_2. These are positively charged cation, which can be combined with negatively charged anion functional groups on graphene oxide. as shown in equation 4.1 and 4.2 [28-30]

$$Ti(OC_4H_9)_4 + 4H_2O \longrightarrow Ti(OH)_4 + 4C_4H_9OH \qquad \text{Equation 4.1}$$

$$Ti(OC_4H_9)_4 + C_2H_5OH \longrightarrow Ti(OC_2H_5)_x(OC_4H_9)_y + C_4H_9OH \quad \text{Equation 4.2}$$

Reaction intermediates; $Ti(OH)_4$ (Equation 4.1) and $Ti(OC_2H_5)_x(OC_4H_9)_y$ (Equation 4.2) were converted into TiO_2 via condensation reaction as shown in equation 4.3 and 4.4 [28-30], and via calcination at high temperature.

$$Ti(OH)_4 + Ti(OC_4H_9)_4 \longrightarrow TiO_2 + C_4H_9OH \quad \text{Equation 4.3}$$

$$Ti(OH)_4 \longrightarrow TiO_2 + 2H_2O \quad \text{Equation 4.4}$$

In the composite material (40wt%TiO_2/rGO) synthesis process, Ti^{4+} and graphene solution were mixed and stirring time was varied at 3,6,12 and 24 hours. Afterward, solutions were calcined at 450 ^oC. TiO_2/rGO (stirring 12 hours) only that can covert CO_2 to ethanol (9.38 μmol/g) because. TiO_2 nanoparticles were agglomerated when using stirring time at 3 and 6 hours as shown in Figure 4.2a and 4.2b, respectively. Less TiO_2 nanoparticles were observed on graphene sheet when 24 hours stirring time was used. Stirring time of 12 hours was determined to be the best condition as shown Figure 4.2c. Increasing the mixing time will result in more $Ti(OC_4H_9)_4$ conversion into Ti^{4+}. However, if duration of mixing is beyond the suitable condition, Ti^{4+} will be converted to TiO_2, forming solid particles along with the effect of centrifugal force, resulting in less amounts of TiO_2 on graphene oxide. The TiO_2 nanoparticles are thoroughly distributed on graphene sheet. This parameter was then used in the synthesis of 10-60 wt% TiO_2/rGO using sol-gel method the presence of Ti was confirmed with EDX spectra in Figure 4.3.

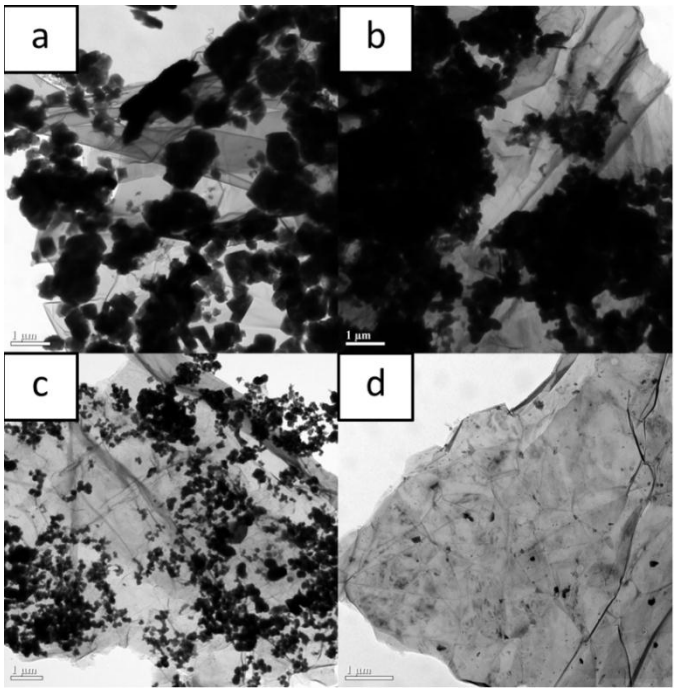

Figure 4.2 TEM images of TiO_2/rGO synthesized with different stirring time at a) 3 hours, b) 6 hours, c) 12 hours and d) 24 hours

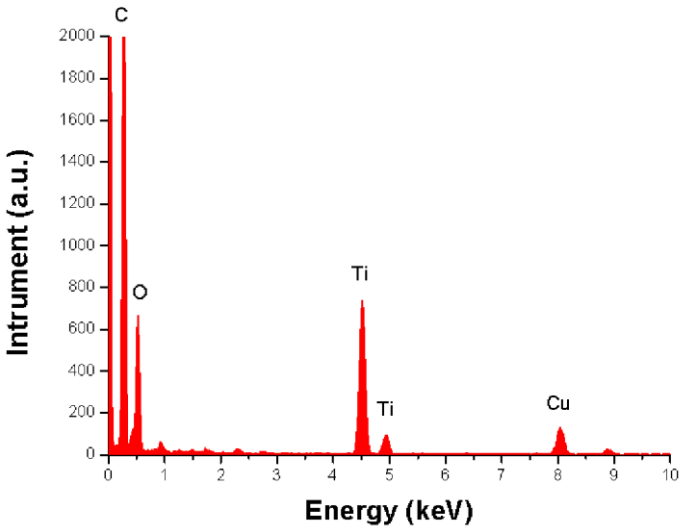

Figure 4.3 EDX pattern of TiO_2/rGO composite

Figure 4.4 shows TEM images of TiO_2/rGO, synthesized under conditions of 10-60 %wt TiO_2 loading. The TiO_2/rGO with 10 wt% TiO_2 loading (Figure 4a) shows only a few TiO_2 nanoparticles attached to graphene sheet, while graphene sheet was fully deposited by TiO_2 in case of 60 wt% TiO_2 loading (Figure 4f). It was

observed in Figure 4.4 that %wt TiO_2 loading affect number and diameter sizes of the TiO_2 nanoparticles. More particles with bigger diameter size were spotted as the TiO_2 loading increased from 10 to 20, 30, 40, 50, and 60 wt. % (Figure 4.4b, 4.4c, 4.4d and 4.4e). This phenomenon addressed good control of our synthesis technique over size and distribution of the TiO_2 nanoparticles.

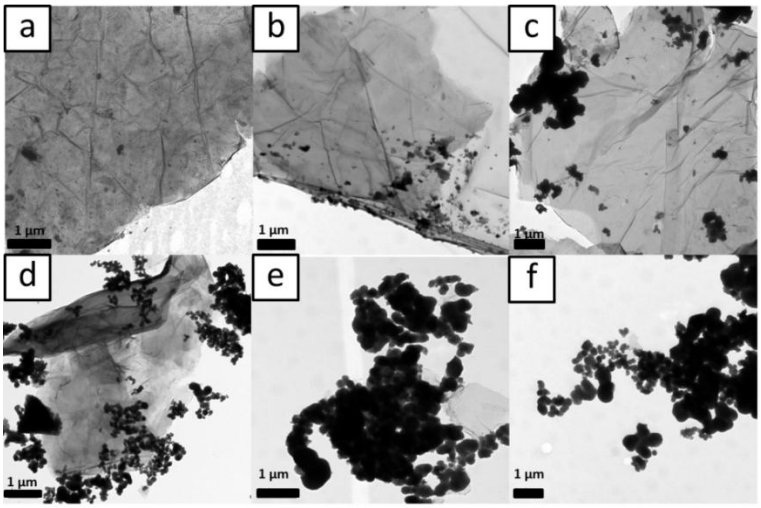

Figure 4.4 TEM images of other TiO_2/rGO a) 10 wt.%, b) 20 wt.%, c) 30 wt.%, d) 40 wt.%, e) 50 wt.%, f) 60 wt.%

4.1.2 CuO-TiO_2/rGO

Chemical deposition and heat treatment were used in the synthesis of CuO-TiO_2/rGO. Firstly, CuO-TiO_2 was synthesized with $Cu(NO_3)_2.5H_2O$ and $Ti(OC_4H_9)_4$ by a chemical deposition method and calcined at 450 ^oC, before mixing the CuO-TiO_2 with GO solution at 120^oC. SEM images (Figure 4.5) as shown the copper nanoparticles attached as small dots on TiO_2 nanoparticles and, both the metal oxides, were anchored on graphene sheets (Figure 4.5b to 4.5f). The CuO-TiO_2 interfaces were maximized while positioned on the graphene support. In possible, doping of CuO is resulting for active site or phase of TiO_2. Because mass of CuO loading have an effect to receive free electron from TiO_2 and cover pore of TiO_2

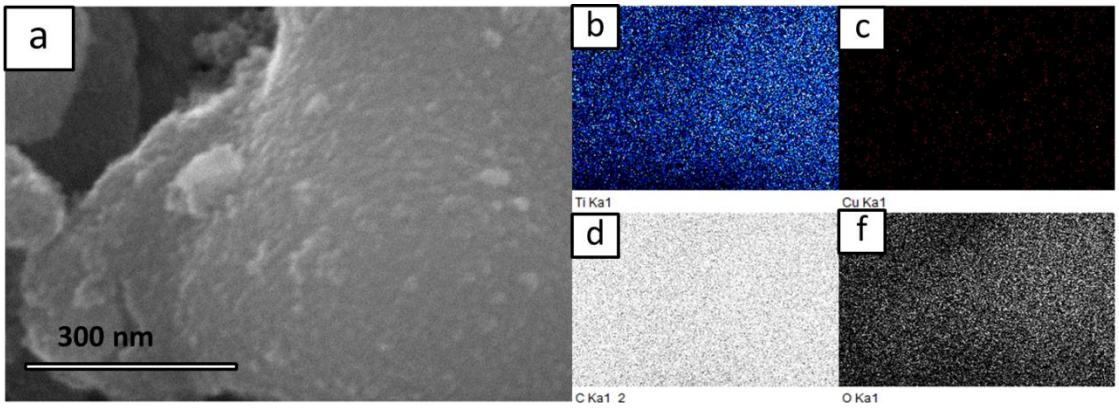

Figure 4.5 a) SEM images of CuO-TiO_2/rGO, b) Titanium mapping, c) copper mapping, d) carbon mapping, f) oxygen mapping

4.2 FTIR analysis

The FTIR spectra (Figure 4.6) show the percentage of light transmittance at wavenumber ranging from 4000 to 400 cm^{-1}. Decrease in %Transmittance due to the absorbed infrared radiation can be correlated to the functional groups on the tested samples. FTIR spectra of GO reveals the presence of hydroxyl group (1056 and 3400, cm^{-1}), carboxylic group (1218 and 1719 cm^{-1}), (1056 cm^{-1}), and aromatic C=C group (1626 cm^{-1}), corresponding to the work of Zhang J. et al. [31]. The FTIR spectra of TiO_2 show one strong peak indicating Ti-O-Ti bonds (604 cm^{-1}). TiO_2/rGO composite spectra also shows a strong peak of Ti-O-Ti and Ti-O-C (596 cm^{-1}), which is an evident for composite formation [32]. The intensity of the carboxyl, hydroxyl, and aromatic peaks of TiO_2/rGO was greatly reduced as the GO was transformed to rGO, a form of graphene oxide with reduced functional groups. This can be attributed to two factors; the chemical reduction of Ti^{4+} and thermal reduction effect, which have a significant effect in partially breaking down the functional groups on the structure of GO. The removal of functional groups on GO, converting to rGO will result in higher electron transfer ability to accommodate for the reaction with CO_2. The CuO-TiO_2/rGO composite was synthesized via the sol-gel method by firstly synthesizing

the CuO-TiO_2 nanoparticles and later introducing the particles to the graphene sheets. In 0.5wt.%CuO-20wt.%TiO_2/rGO and 0.5wt.%CuO-20wt.%P25/rGO (dot-dash line), Ti-O-Ti/Cu-O composite shows a strong peak at 524 cm^{-1} [33], but was not well indicated in our case due to signal suppression from GO.

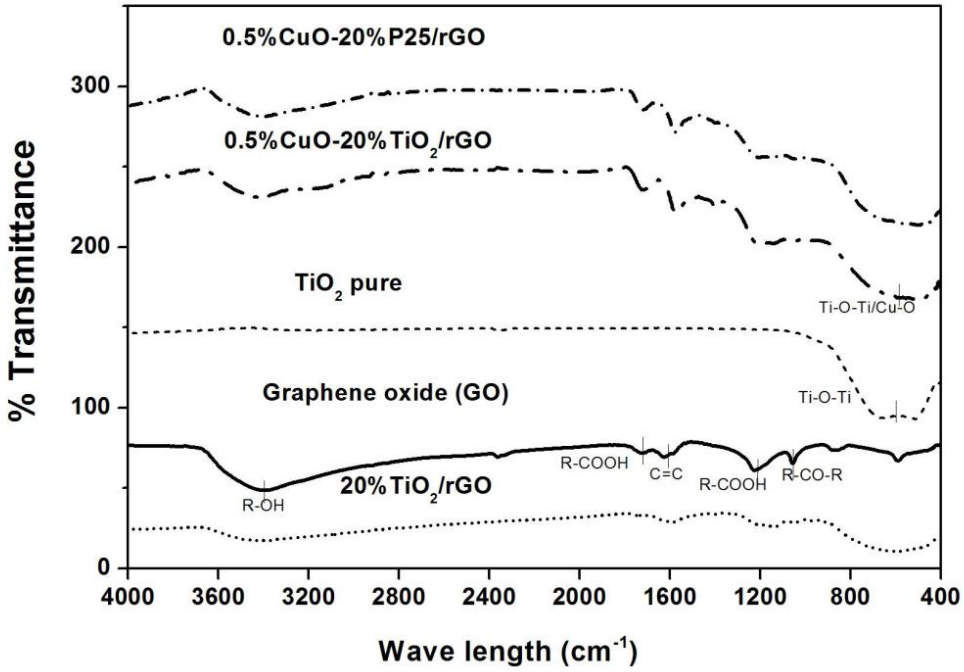

Figure 4.6 FTIR spectra of GO, TiO_2, TiO_2/rGO and CuO-TiO_2/rGO

4.3 XRD analysis

XRD patterns of pure TiO_2 (from sol-gel method) is shown in is shown in Figure 4.7. Peaks at 25.48°, 37.85°, 48.32° and 62.74° are in conformity with database for the TiO_2 anatase phase (101, 004, 200, 211, and 204) [34]. The rutile phase was not found. The signal of TiO_2/rGO also presents the anatase-phase like TiO_2. The XRD spectrum of TiO2/rGO shows good similarity to the anatase phase of TiO_2. Average crystallize size has been estimated by Debye-Scherer formula equation.

$$D = 0.9\lambda/\beta\cos\theta \qquad \text{Equation 4.5}$$

Where, λ is wave length of X-Ray (0.1540 nm), β is full width at half maximum, θ is diffraction angle and D is particle diameter size TiO_2 and TiO_2/rGO

exhibit particle size of 75.51 and 46.69 Å, respectively as shown in the table 4.1. The peak of CuO did not present in the XRD pattern of the CuO-TiO_2/rGO sample due to low amount of copper loading (0.3-2.0 wt.%). However, the present of Cu can be confirmed previously using EDX. XRD pattern also reveal the shift of anatase TiO_2 phase (101) with copper loading and the disappearance of (004), (200), and (204) peaks. This is due to the surface of TiO_2 being covered with CuO, which interfere with the TiO_2 lattice [35], and changes the reflux value of the x-ray spectra. It was determined that 0.5wt.%CuO-20wt.%P25/rGO and 0.5wt.%CuO-20wt.%TiO_2/rGO exhibit particle size of 33.98 and 35.31 Å, respectively as shown in the table 4.1. In addition, the XRD patterns reveal that TiO_2 is in the phase of anatase, which was previous reported by Mino L. et al. to be reactive to CO_2[36]. Moreover anatase phase is high surface area As a result to yield of production.

Table 4.1 Average crystallite size of catalysts

Catalysts	Average crystallize size (nm)
TiO_2	75.51
20wt.%TiO_2/rGO	46.69
0.5wt.%CuO-20wt.%TiO_2/rGO	35.31
0.5wt.%CuO-20wt.%P25/rGO	33.98

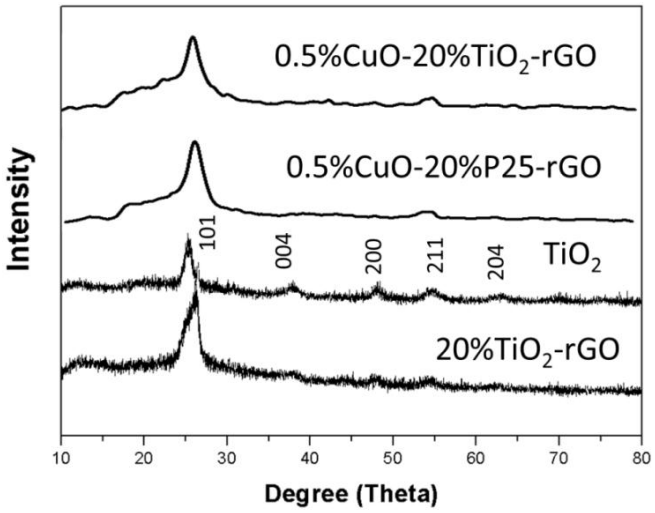

Figure 4.7 XRD patterns of GO, TiO_2, TiO_2/rGO and CuO-TiO_2/rGO

4.4 BET analysis

The material was surface area (multipoint BET) and pore volume (DR method) was reported in Table 4.2. The wt. % of TiO_2 on graphene has an effect on the BET surface as shown in Table 4.2. As wt. % of TiO_2 loading increases, surface area increases up until wt. % TiO_2 loading reaches 50 wt. % (148.2 m^2/g). Surface area seems to decrease after that, resulted from overgrown of TiO_2 nanoparticles to microstructures on graphene sheet.

The wt. % of CuO on TiO_2/rGO also has an effect on the BET surface. Surface area increase with wt. % of CuO until the CuO loading reaches 0.5 wt. % (88.78 m^2/g), in which the surface area begins to decrease. Pore volume also increases until wt% TiO_2 loading reaches 40 wt. % (0.0709 cc/g). The wt% of CuO on TiO_2/rGO also has an effect on the pore volume. Pore volume also increase with %wt of CuO until the CuO loading reaches 0.5 wt. % (0.0398 cc/g), in which surface area begins to decrease. In synthesis of CuO-P25 process, Ultrasonic was applied as mixing $Cu(NO_3)_2$ solution and P25, and provide CuO nanoparticles forming in the P25 pore. The growing of CuO in pore induces the decrease of pore volume and surface area. the pore diameter size of TiO_2 and P25 are similar. P25 has higher pore volume than TiO_2 (sol-gel), resulting in a higher number of pore in P25 than in TiO_2. Therefore, CuO nanoparticles might be formed inside the P25 pore more readily than in the TiO_2 (sol-gel) pore, which decrease the pore volume and surface area of 0.5CuO-20wt%P25/rGO compare to 0.5wt%CuO-20wt%TiO_2/rGO.

Table 4.2 BET surface of catalysts at different wt% CuO and TiO_2 loading

Catalysts	Surface area (m^2/g)	Pore volume (cc/g)
rGO	5.48	0.0022
TiO_2 loading		
10wt.%TiO_2/rGO	97.97	0.0469
20wt.%TiO_2/rGO	106.50	0.0559
30wt.%TiO_2/rGO	117.17	0.0570
40wt.%TiO_2/rGO	144.30	0.0709
50wt.%TiO_2/rGO	148.20	0.0675
60wt.%TiO_2/rGO	127.70	0.0614
TiO_2*	9.81	0.0042
P25**	66.35	0.0294
20wt.%P25/rGO	31.28	0.0134
CuO loading		
0.3wt.%CuO-20wt.%TiO_2/rGO	40.19	0.0182
0.5wt.%CuO-20wt.%TiO_2/rGO	88.78	0.0398
1.0wt.%CuO-20wt.%TiO_2/rGO	24.83	0.0107
2.0wt.%CuO-20wt%TiO_2/rGO	24.00	0.0108
0.5wt.%CuO-20wt.%P25/rGO	22.23	0.0091

*DA Method pore diameter 18.40 Å
**DA Method pore diameter 18.20 Å

4.5 Energy band gap analysis

Energy band gap is a minimum amount of energy required to activate electrons, moving from valence to conductive band. Basic methods for band gap determination includes “Tauc plot” of correlation of UV light absorbance and band gap energy (equation 2.4). Light absorbance value of the composite (in the range of 250-800 nm) was calculated as the α value (equation 2.5) and the relation of $(\alpha hf)^2$ vs hf was plotted (Figure 4.8). Energy band gaps of the TiO_2/rGO composite, shown in table 4.3, reveals changes in optical and electrical properties as a function of wt% of metal loading (TiO_2, CuO) on graphene sheet. As wt. % of metals oxide loading increases, energy band gaps of the material also decrease and eventually plateau [37]. Overloading of metal on graphene will result in more metal nanoparticles covering the surface of composite therefore increasing the energy band gap value. Noting that the

changes in band gap value occurred even at 10wt. % TiO_2 on rGO, hinting interactions/reactions between titanium and graphene carbon on the composite materials. It is possible that direct contact between titanium and graphene is required to alter the band gap of the composite material, and that overgrowth TiO_2 on TiO_2 (not graphene) contributes no effect on the band gap value.

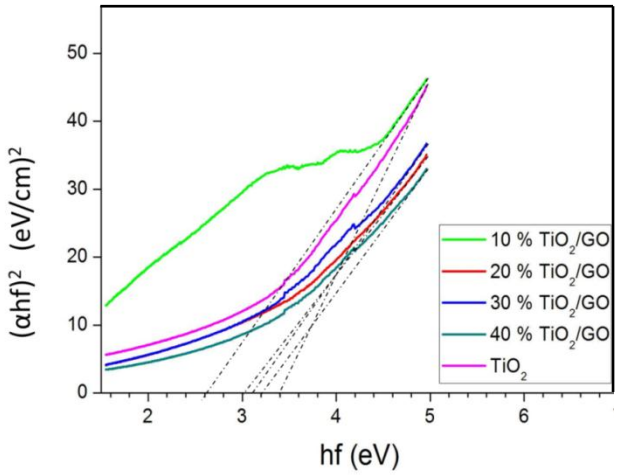

Figure 4.8 Tauc plot of TiO_2/rGO and TiO_2

Table 4.3 Energy band gap value of metal oxide composite graphene

Catalysts	Energy band gap (eV)
rGO	3.4
TiO_2 loading	
10wt.%TiO_2/rGO	2.6
20wt.%TiO_2/rGO	3.1
30wt.%TiO_2/rGO	3.2
40wt.%TiO_2/rGO	3.2
50wt.%TiO_2/rGO	3.4
60wt.%TiO_2/rGO	3.5
TiO_2	3.1
P25	3.1
CuO loading	
0.3wt.%CuO-20wt.%TiO_2/rGO	3.0
0.5wt.%CuO-20wt.%TiO_2/rGO	3.1
1.0wt.%CuO-20wt.%TiO_2/rGO	3.2
2.0wt.%CuO-20wt.%TiO_2/rGO	3.3
20wt.%P25/rGO solgel 120^{o}C	3.2
0.5wt%CuO-20wt.%P25/rGO	3.2

4.6 Effect of TiO_2 loading on production yield

In this case, it was believed that photocatalytic reaction occurred mainly on TiO_2, and that graphene was needed to support the TiO_2 catalyst and to provide desired protons and electrons to the reaction [37]. Energy band gaps of GO, TiO_2/rGO with different amount of TiO_2 loading, and TiO_2 were obtained from plots of UV-visible adsorption spectra (α) and light energy (electron volts, eV) (Tauc plot, Figure 4.9) while solid surface area of the materials were acquired using BET surface analyzer (Autosorb). Figure 4.9 shows the ethanol yield of GO, TiO_2, and TiO_2/rGO photo-catalysts with increasing value of titanium loading. The composite material (TiO_2/rGO) has a higher production yield than GO and TiO_2, which can be attributed to four reasons; First, the high specific surface area of GO helps increase CO_2 adsorption and activation. Second, GO can absorb light in the visible and UV-visible wavelength resulting in higher efficiency of TiO_2/rGO than TiO_2 and GO. Third, functional groups of GO can act as capping agent which help limit the growth and reduce the agglomeration of nanoparticles. Finally, energy band gap of TiO_2 was reduced by GO because of the enhanced electron conductivity of GO [38]. XRD patterns (Figure 4.7) reveal that TiO_2 has anatase phase. Mino L. et al. [36] have suggested that CO_2 is absorbed on the anatase phase of TiO_2 (101).

In the CO_2 conversion experiments, some condition have low production yield (Area under the ethanol peak is lower than the accepted limit of detection of gas chromatography). The 20 wt. % TiO_2/rGO composite exhibited relatively the highest photocatalytic activity, yielding ethanol concentration at 28.62 μmoles ethanol per gram composite. High performance from 20 wt. % TiO_2/rGO was achieved due to combined effects of low band gap energy (2.9 eV), and high surface area (106.5 m^2/g). As presented in Table 2 and Table 3, the sample with 10 wt. % TiO_2/rGO exhibited a lower energy band gap (2.6 eV) but lower surface area when compared to 20 wt. % TiO_2/rGO. 20 wt. %TiO_2/rGO, As increasing TiO_2 loading (20-60 wt. %), not only the surface are increase but also energy band gap. This caused the reduction in ethanol yield. Metal loading higher than 20wt% will result in excessive amount of TiO_2 covering the active site area (composite area), which will lower the ethanol yield. Moreover metal loading higher than 20wt% has a higher energy band gap than 20 wt. % TiO_2/rGO

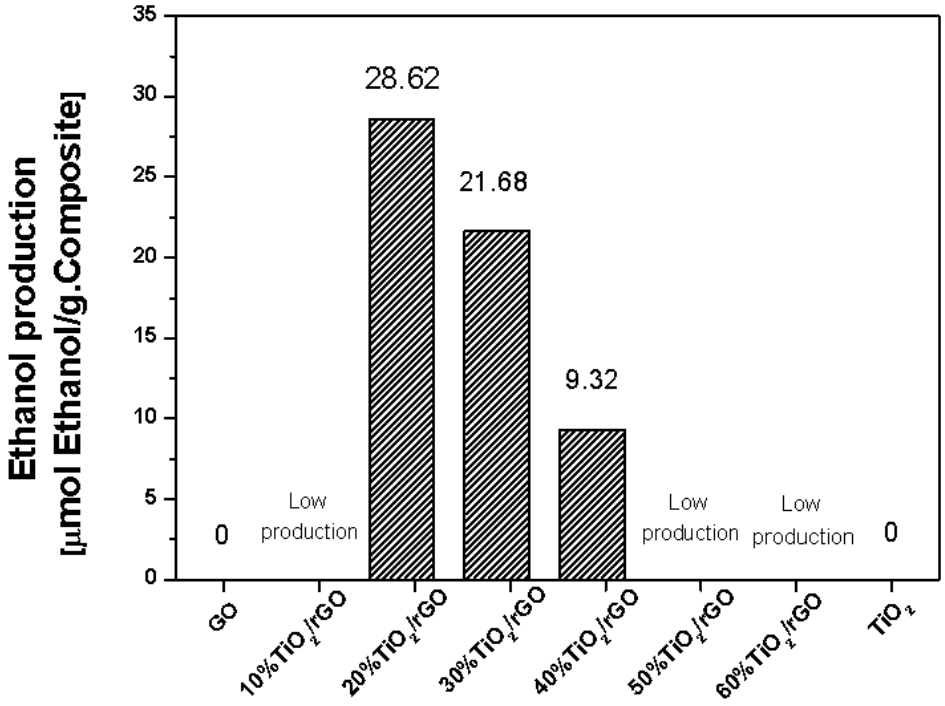

Figure 4.9 Ethanol productions that corresponded to TiO_2 loading on composite

The energy conduction band of TiO_2 anatase (4.25 eV) has a higher E_{NHE} than graphene (4.42 to 4.5 eV.) [39-41], so it enables the transfer of electrons from TiO_2 to graphene sheet. Graphene can then provide a large active site for photocatalytic reaction of CO_2 as shown in Figure 4.10-4.11. So this provides a higher active site for photoreaction of CO_2 than pure TiO_2.

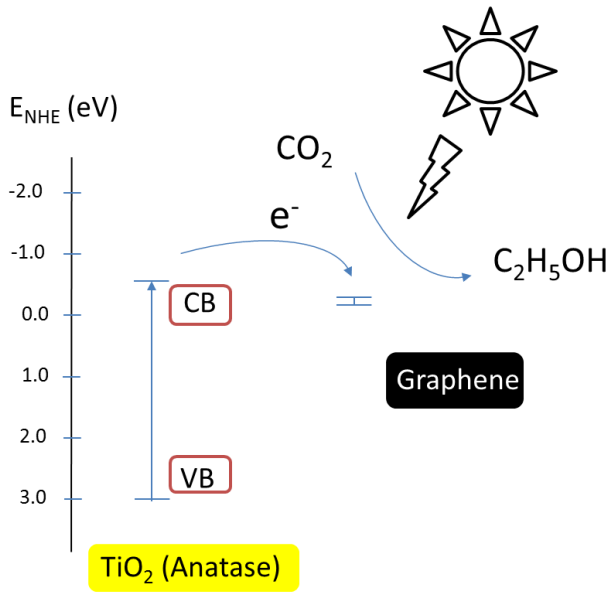

Figure 4.10 Charge transfer processes occurring on the exposed TiO_2/rGO

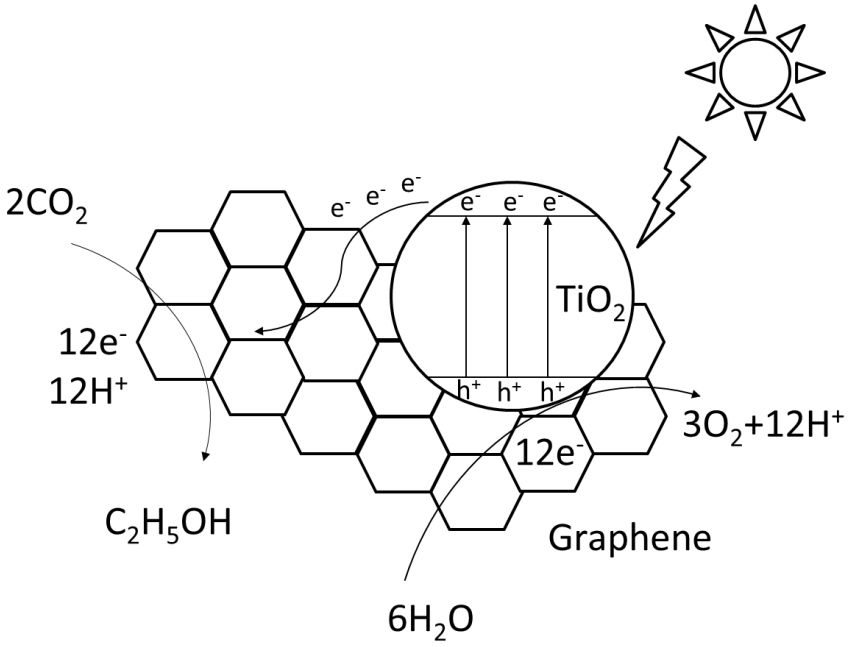

Figure 4.11 Reaction mechanism in the photoreduction of CO_2 (TiO_2/rGO)

4.6.1 Effect of comparison TiO_2 & P25

TiO_2 commercial grade (P25, Aeroxide) composite graphene was prepared by sol-gel method (mixing 12 hours). Ethanol yield from 20wt%P25/rGO is zero. There is a possibility that P25 has some functional groups or/and chemical coated on the surface to reduce particle agglomeration, which hinder the nanoparticles formation on the surface of rGO. In sol-gel at 120^{o}C, after adding P25 in graphene solution, the mixer was heated to 120 ^{o}C and maintain for 1 hour. In this process, thermal effect might be able to remove some functional groups or/and chemical which hinder particle formation on surface of P25, resulting in a high solubility of P25 in ethanol/water and physic adsorption between GO and P25 as shown in Figure 4.13. In this case, 20wt%P25/rGO lower ethanol production yield than P25 pure because the P25 is a material high surface area (66.35 m^2/g) and pore volume (0.0294 cc/g) [40]. Doping P25 in to GO, which cover surface area and pore volume of P25 as shown in Table 4.2 (20wt. %P25/rGO)

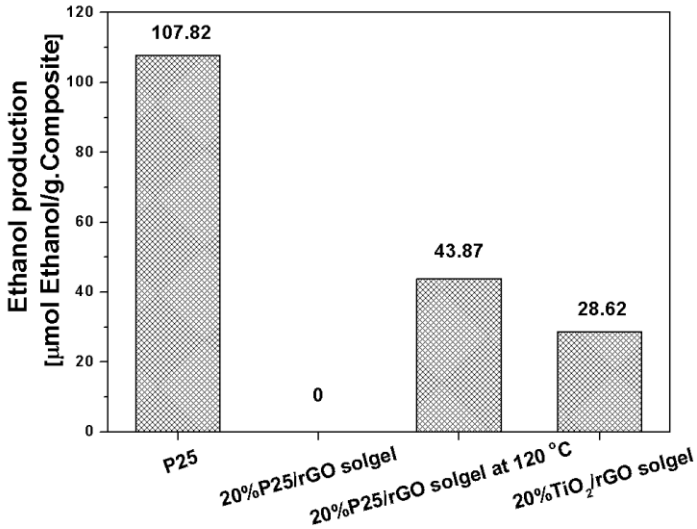

Figure 4.12 Ethanol productions that corresponded to P25 loading on composite

4.7 Effect of CuO loading on production yield

CuO-TiO_2 was synthesized by sol-gel method then it was added in graphene solution under stirring and heated to 120 ^{o}C. From Figure 4.14, CuO-TiO_2/rGO has a higher ethanol production yield than that of the TiO_2/rGO due to the presence of CuO and CuO/TiO_2 enhance the CO_2 adsorption ability [36,42,43].

Moreover, CO_2 is absorbed by Cu^+/TiO_2 and H^+ is accepted by Cu^+ reform to Cu^{2+} again respectively [5,43] (Equation 4.11 to 4.13) resulting $CuO\text{-}TiO_2$/rGO high active site area than TiO_2/rGO

$$TiO_2 \longrightarrow e^-_{cb}\,(TiO_2) + H^+_{vb}(TiO_2) \qquad \text{Equation 4.11}$$

$$Cu^{2+} + e^- \longrightarrow Cu^+ \qquad \text{Equation 4.12}$$

$$Cu^+ + H^+ \longrightarrow Cu^{2+} \qquad \text{Equation 4.13}$$

The 0.5wt.%CuO-20wt.%TiO_2/rGO offers the highest ethanol production yield (162.67 µmol/g). The optimization of %wt copper loading to ethanol production yield can be attributed from BET surface area (Table 4.1). If the copper loading exceed 0.5 %wt, ethanol production yield will decrease. This is resulted from higher amount of CuO which cover the surface of TiO_2 interrupting the photocatalytic reaction of CO_2 as shown in Figure 4.13.

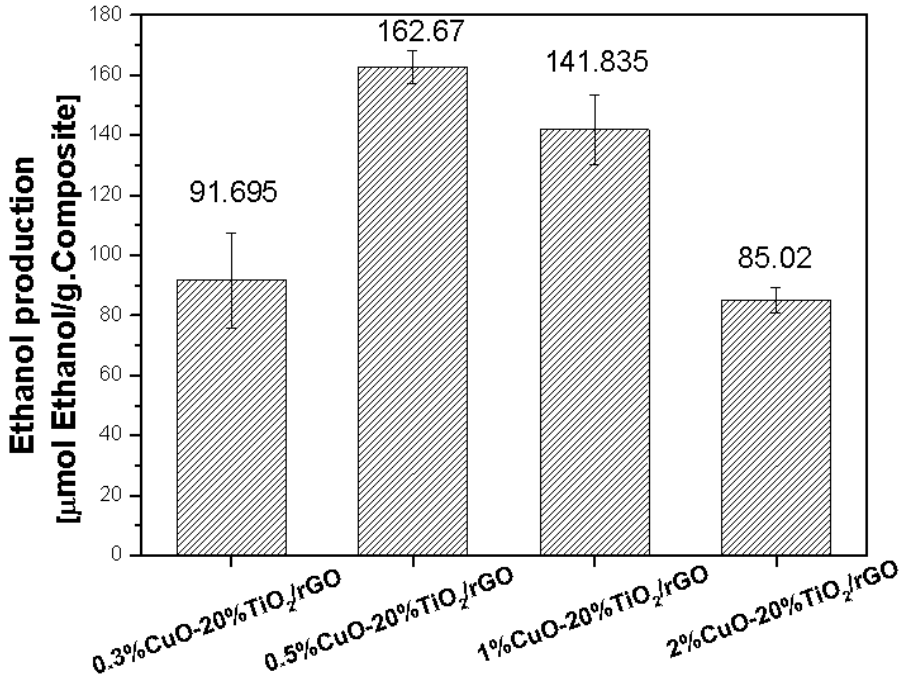

Figure 4.13 Ethanol productions that corresponded to CuO loading on composite

E_{NHE} of graphene has value between 4.42 to 4.5 eV. The conduction band of TiO_2 (anatase) has a higher E_{NHE} than graphene and CuO respectively [39-41]. In Figure 4.14-4.15, electrons from TiO_2 can be transferred to graphene sheet and CuO.

The addition of CuO will increase the active site area of the composite, resulting in higher ethanol yield with CuO-TiO_2/rGO compare to TiO_2/rGO.

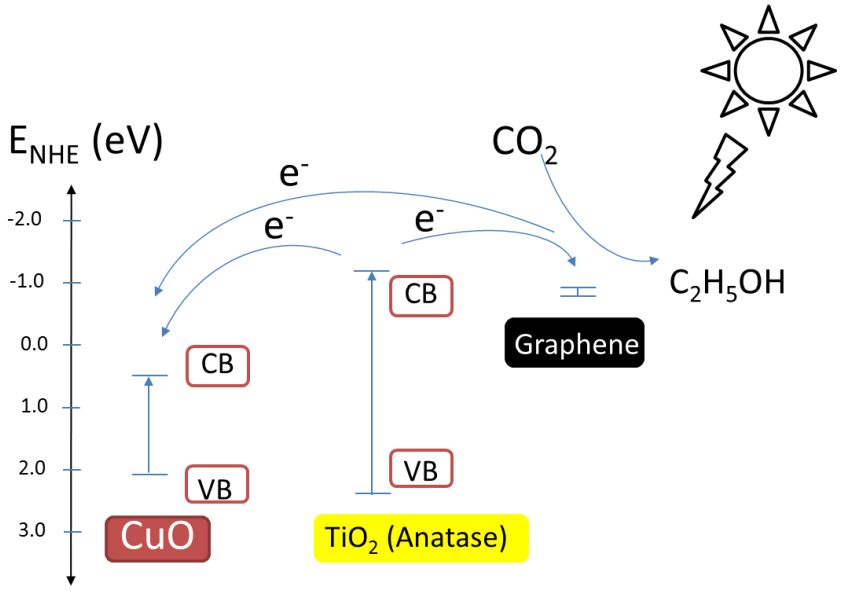

Figure 4.14 Charge transfer processes occurring on the exposed CuO-TiO_2/rGO

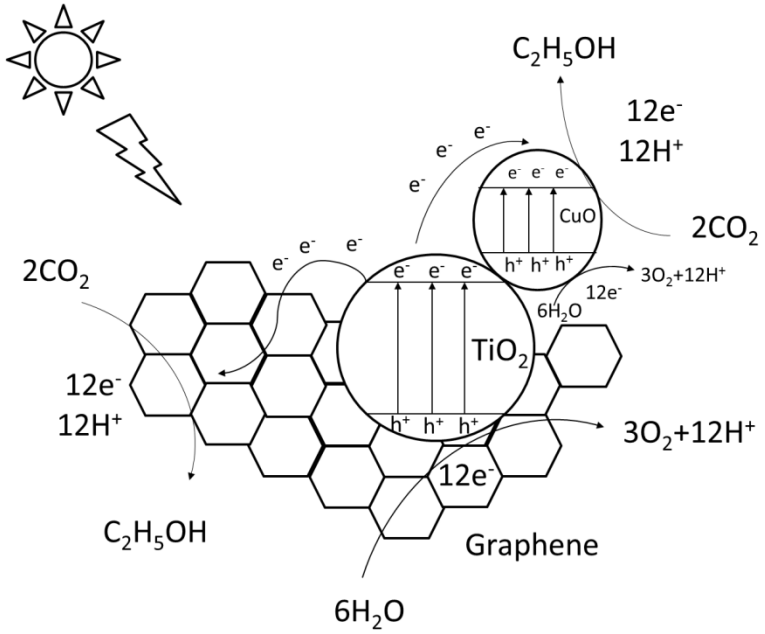

Figure 4.15 Reaction mechanism in the photoreduction of CO_2 (CuO-TiO_2/rGO)

4.7.1 Effect of comparison Cu-TiO_2 , CuO-P25 on graphene

The best condition (0.5CuO-20%TiO_2/rGO) was compared with 0.5CuO-20wt%P25/rGO in regarding to the production yield of ethanol in Figure 4.16. 0.5CuO-20wt%P25/rGO has a lower production yield than 0.5wt%CuO-20wt%TiO_2/rGO due to the lower surface area of 0.5wt%CuO-20wt%P25/rGO compare to 0.5wt%CuO-20wt%TiO_2/rGO. In synthesis of CuO-P25 process, Ultrasonic was applied as mixing $Cu(NO_3)_2$ solution and P25, and provide CuO nanoparticles forming in the P25 pore. The growing of CuO in pore induces the decrease of pore volume and surface area. Therefore, the active site of CuO is significantly reduced [44]. CuO is unable to receive the UV-visible light, which is necessary to convert CO_2 into ethanol. From BET analysis data (Table 4.1), the pore diameter size of TiO_2 and P25 are similar. P25 has higher pore volume than TiO_2 (sol-gel), resulting in a higher number of pore in P25 than in TiO_2. Therefore, CuO nanoparticles might be formed inside the P25 pore more readily than in the TiO_2 (sol-gel) pore, which decrease the pore volume, surface area and active site area of 0.5CuO-20wt%P25/rGO compare to 0.5wt%CuO-20wt%TiO_2/rGO.

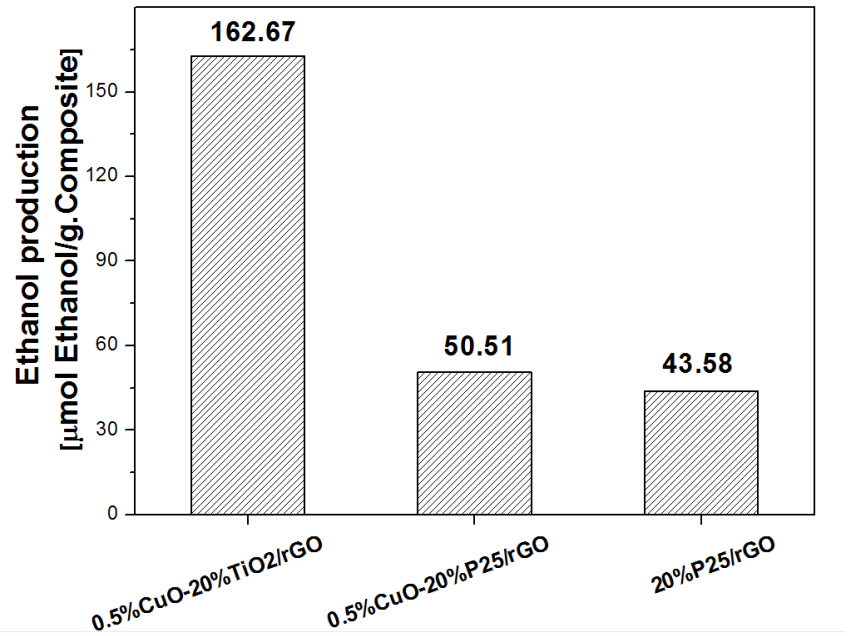

Figure 4.16 Ethanol productions of 0.5wt.%CuO-20wt.%TiO_2/rGO, 0.5wt.%CuO-20wt.%P25/rGO, and 20wt. %P25/rGO

CHAPTER V
CONCLUSION

Physical and chemical properties characterizations revealed that TiO_2 was in anatase phase, and was successfully deposited on graphene surface in the form of amorphous shaped nanoparticles with particle size ranging from 8-10 nm. During the experiment, CO_2 is fed continuously into the photo-reactor containing the photo-catalyst at a rate of 100 ml/min for 12 hours. Inside the reactor, CO_2 is dispersed in water and is exposed to light in the visible and ultraviolet wavelength from the 160 W mercury lamp. The optimal wt%TiO_2 loading of TiO_2/rGO for ethanol production is 20wt%, yielding 28.62 µmol of Ethanol per grams composite catalyst, which is a combined effect of low band gap energy and high surface area. However, bimetallic copper-titanium graphene composite (CuO-TuO_2/rGO) showed even better performance in converting CO_2 to ethanol. The highest recorded ethanol yield was 162.67 µmol Ethanol per gram catalyst from The 0.5wt%CuO-20wt%TiO_2/rGO. This process reveals the potential of TiO_2/rGO and CuO-TiO_2/rGO as photo-catalyst which can produce ethanol from CO_2 at low temperature and atmospheric pressure.

Suggestions

1. Other methods of TiO_2 synthesis such as thermal and co-precipitate method should be explored as viable options for the synthesis of composite material.

2. The photocatalytic reactor can be improved to enhance the ethanol production yield. For example;

-The light source for photocatalytic reaction can be applied more efficiently by redesigning the reactor to a tubular reactor design.

-An ultrasonic wave can be used composite catalyst and active radicals to ensure an even better contact between the

REFERENCES

1 zfacts. Evidence that CO_2 is Cause.[serial online].Available from**:** http://zfacts.com/p/226.html.Accessed July 1, 2016.

2 National Institute for Occupational Safety and Health. The Emergency Response Safety and Health Database: Methanol.[serialonline]. Available from: http://www.cdc.gov/niosh/ershdb/EmergencyResponseCard _29750029.html.Accessed July 1, 2016.

3 Reel M. Brazil's Road to Energy Independence.[serial online]. Available from: http://www.washingtonpost.com/wpdyn/content/article/2006/08/19/AR20 06081900842.html.Accessed July 1, 2016.

4 Li K., An X., Park K.H., Khraisheh M., Tang J. (2014). A critical review of CO_2 photoconversion: Catalysts and reactors. Catalysis Today ,224, 3–12.

5 Slamet, Nasution H.W., Purnama E., Kosela S. and Gunlazuardi J (2005).Photo-catalytic reduction of CO_2 on copper-doped Titania catalysts prepared by improved-impregnation method.Catalysis Communications,6,313-319

6 Liu E., Hu Y., Li H., Tang C.,Hu X.,Fan J.,Chen Y.,Bian J (2015). Photoconversion of CO_2 to methanol over plasmonic Ag/TiO_2 nano-wire films enhanced by overlapped visible-light-harvesting nanostructures. Ceramics International,41,1049–1057.

7 Koci K., Mateˇju K., Obalova L., Krejcˇikova S., Lacny´ Z., Placha D., Cˇapek L.,Hospodkova A.,Solcova O (2010). Effect of silver doping on the TiO_2 for photocatalytic reduction of CO_2. Applied Catalysis B: Environmental, 96, 239–244

8 Hummer S. W., Offeman E.R (1957). Preparation of Graphitic Oxide.journal of the American chemical society, 80(6), 1339

9 Zhao Y., Zhao D., Chen C., Wang X (2013). Enhanced photo-reduction and removal of Cr(VI) on reduced graphene oxide decorated with TiO_2 nanoparticles. Journal of Colloid and Interface Science, 405, 211–217

10 Shaw M. Carbon Dioxide (CO_2) - A Greater Hazard Than Often Considered. [serial online].Available from:http://www.cacgas.com.au/blog/bid/383463/Carbon-Dioxide-CO2-A-Greater-Hazard-Than-OftenConsidered.Accessed July 5,2016

11 Al-Mayouf A (2015). Metal oxides as photocatalysts. Journal of Saudi Chemical Society, 5(19), 462–464

12 Rochelle G.T. (2009). Amine scrubbing for CO_2 capture. Science 325 (5948),1652-1654

13 Liu Y. Huang B., Dai Y., Zhang X., Qin Xia a, Jiang M., Whangbo M.H. (2009).Selective ethanol formation from photocatalytic reduction of carbon dioxide in water with $BiVO_4$ photocatalyst. Catalysis Communications, 11 ,210–213

14 Chang X., Wang T., Gong J (2016). CO_2 photo-reduction: insights into CO_2 activation and reaction on surfaces of photocatalysts. Energy &Environmental Science,9,2177-2196

15 Department of Physics and Astronomy (Georgia University). Band theory of solid [serial online]. Available from:http://hyperphysics.phyastr.gsu.edu/hbase/solid/band.htlm.Accessed May 5,2016

16 Narayanan R., Deepa M., and Srivastava A.K. (2011). Nanoscale Connectivity in a TiO_2/CdSe Quantum Dots/Functionalized Graphene Oxide Nanosheets/Au Nanoparticles Composite for Enhanced Photoelectrochemical Solar Cell Performance. *Phys Chem Chem Phys,4(2),767-778.*

17 Hsu H.C, Shown I., Wei H.Y., Chang Y.C., Du H.Y., Lin Y.G., Tseng C.A., Wang C.H., Chen L.C.,Lin Y.C.,Chen K.H. (2013).Graphene oxide as a promising photocatalyst for CO_2 to methanol conversion.Nanoscale,5,262-268

18 Sritawong T .Titanium: Photocatalytic [serial online].Available from**:** http://www.vcharkarn.com/varticle/27809.Accessed May 25,2016

19 Go´rska P., Zaleska A., Kowalska E.,Klimczuk T.,Sobczak J.W., Skwarek E.,Janusz W.,Hupka J(2008). TiO_2 photoactivity in vis and UV light: The influence of calcination temperature and surface properties.Applied Catalysis B: Environmental,84, 440–447

20 Rajalakshmi K., Jeyalakshmi V., Krishnamurthy K.R.; Viswanathan B (2012).Photocatalytic reduction of carbon dioxide by water on titania: Role of Photophysical and structucral properties. Indian journal of chemistry, 51(2), 411-419

21 Oluwafunmilola O., Mercedes M.V. (2015). Review of material design and reactor engineering on TiO_2 photocatalysis for CO_2 reduction. Journal of Photochemistry and Photobiology C: Photochemistry Reviews, 24, 16–42

22 Liu E., Hu Y., Li H., Tang C., Hu X., Fan J., Chen Y., Bian J(2015). Photoconversion of CO_2 to methanol over plasmonic Ag/TiO_2 nano-wire films enhanced by overlapped visible-light-harvesting nanostructures.Ceramics International, 41, 1049–1057

23 Koci K., K.Mateˇju K., Obalova L., Krejcˇikova S., Lacny´ Z., Placha D., Cˇapek L.,Hospodkova A.,Solcova O (2010). Effect of silver doping on the TiO_2 for photocatalytic reduction of CO_2. Applied Catalysis B: Environmental, 96, 239–244

24 Wang A., Li X., Zhao Y. ,Wu W., Chen J., Meng H (2014). Preparation and characterizations of Cu_2O/reduced graphene oxide nanocomposites with high photo-catalytic performances. Powder Technology, 261, 42-48

25 Li X., Wang Q., Zhao Y. ,Wu W., Chen J., Meng H (2013). Green synthesis and photo-catalytic performances for ZnO-reduced graphene oxide nanocomposites. Journal of Colloid and Interface Science,411, 69–75

26 Zhang Q., Lin C.F.,Jing Y.H.,Chang C.H.(2013). Photocatalytic reduction of carbon dioxide to methanol and formic acid by graphene-TiO_2.Journal of the Air & Waste Management Association, 64, 578-585

27 Liu J., Niu Y., He X., Qi J.,Lin X(2016). Photocatalytic Reduction of CO_2 Using TiO_2-Graphene Nanocomposites. Journal of Nanomaterials,23,245-250

28 Honda H., Suzaki K.,Sukahara Y.(2000). Control of Hydrolysis and Condensation Reactions of Titanium tert-butoxide by Chemical Modification with Catechol**.** Journal of Sol-Gel Science and Technology,22,133-138

29 Hirai T., Sato H., Komasawa I (1993). Mechanism of Formation of Titanium Dioxide Ultrafme Particles in Reverse Micelles by Hydrolysis of Titanium Tetrabutoxide Ind. Eng. Chem. Res.,32,3014-3019

30 Simonsen M.E., Sogaard E.G (2010). Sol–gel reactions of titanium alkoxides and water: influenceof pH and alkoxy group on cluster formation and properties of the resulting products**.** Journal of Sol-Gel Science and Technology,53,485-497

31 Zhang J., Yang H.Shen G.,Chen P., Guo S (2009). Reduction of graphene oxide via L-ascorbic acid.ChemComm,46,1112-1114

32 Tan L., Ong- W.J., Chai S.P., Mohamed A.R(2013). Reduced graphene oxide-TiO_2 nanocomposite as a promising visible-light-active photocatalyst for the conversion of carbon dioxide. Nanoscale Research Letters,8,789-799

33 Fang Y., Wang R., Jiang G., Jin H., Wang Y., Sun X., Wang S., Wang T (2012). CuO/TiO_2 nanocrystals grown on graphene as visible-light responsive photocatalytic hybrid materials.Mater. Sci ,35, 495–499

34 Dos Santo J. G., Ogasawara T., Corrêa R. A(2009). Synthesis of mesoporous titania in rutile phase with pore-stable structure. Brazilian Journal of Chemical Engineering,26,555 – 561

35 Chen B.R., Nguyen V.H., Wu J., Martin R., Kocˇı´ K. Production of renewable fuels by the photohydrogenation of CO_2: effect of the Cu species loaded onto TiO_2 photocatalysts .Phys.Chem.Chem.Phys,18, 4942-4951

36 Mino L., Spoto G., Ferrari A.M(2014). CO_2 Capture by TiO_2 Anatase Surfaces: A Combined DFT and FTIR Study. J. Phys. Chem,118, 25016−25026

37 Saleem H., Habib A(2016). Study of band gap reduction of TiO_2 thin films with variation in GO contents and use of TiO_2/Graphene composite in hybrid solar cell. Journal of Alloys and Compounds,679,177-183

38 Low J., Yu J., Ho W(2015). Graphene-Based Photocatalysts for CO_2 Reduction to Solar Fuel. American Chemical Society,6, 4244−4251

39 Kumar S.P., Sundaramurthy J., Sundarrajan S., Babu V.J., Singh G., Allakhverdiev

S.I., Ramakrishna S (2014). Hierarchical electrospun nanofibers for energy harvesting, production and environmental Remediation. Energy&Environmental Science,7, 3192–3222

40 Adán-Más A., Wei D. (2013), Photoelectrochemical Properties of Graphene and Its Derivatives.Nanomaterials,3,325-356

41Wang G., Xu L., Zhang J.,Yin T.,Han D (2013). CuO_x– TiO_2 junction: what is the active component for photocatalytic H_2 production?. Phys.Chem. Chem. Phys, 15, 14956-14960

42.Peng M.M., Hemaltha P., Ganesh M. Vinodh R.,Jang H.T(2013).Synthesis and Characterization of Novel Mesoporous CuO and Its Application to CO_2 Capture,27(15), 9941-9944

43 Liu L., Zhao C., Li Y(2012). Spontaneous Dissociation of CO_2 to CO on Defective Surface of Cu(I)/TiO_{2-x} Nanoparticles at Room Temperature. The Journal of Physical Chemistry,116, 7904−7912

44 Liu L., Zhao C., Miller J.T., Li Y(2016). Mechanistic Study of CO_2 Photoreduction with H_2O on Cu/TiO_2 Nanocomposites by In Situ X-ray Absorption and Infrared Spectroscopies. The Journal of Physical Chemistry,121(1), 490–499

APPENDICES

APPENDIX A

Calculate for metal loading production

-In 20%wtTiO_2/rGO condition; Using GO 0.1 gram

$$\frac{\text{Mass of Ti}}{0.1 + \text{Mass of Ti}} \times 100 = 20$$

$$\text{Mass of Ti} = 0.2(0.1 + \text{Mass of Ti})$$

$$\text{Mass of Ti} = 0.025 \text{ gram}$$

M.W. $_{Ti(OC4H9)4}$ = 340.32 gram/mol, M.W. $_{Ti}$ = 47.86 gram/mol

$$Ti(OC_4H_9)_4 \longrightarrow Ti$$

$$\text{Mol of } Ti(OC_4H_9)_4 = \text{ Mol of Ti}$$

$$\frac{\text{Mass of Ti(OC4H9)4}}{340.32 \text{ gram/mol}} = \frac{\text{Mass of Ti}}{47.86 \text{ gram/mol}}$$

$$\frac{\text{Mass of Ti(OC4H9)4}}{340.32 \text{ gram/mol}} = \frac{0.025 \text{ gram}}{47.86 \text{ gram/mol}}$$

$$\text{Mass of } Ti(OC_4H_9)_4 = 0.18319 \text{ gram}$$

-In 0.5CuO%wt-20%wtTiO_2/rGO condition; Using GO 0.1 gram

$$\frac{\text{Mass of Cu}}{0.1 + \text{Mass of Ti} + \text{Mass of Cu}} \times 100 = 0.5$$

$$\frac{\text{Mass of Cu}}{0.1 + 0.025 + \text{Mass of Cu}} \times 100 = 0.5$$

$$\text{Mass of Cu} = 5\times10^{-3}(0.1 + 0.0025 + \text{Mass of Cu})$$

$$\text{Mass of Cu} = 5.15\times10^{-4} \text{ gram}$$

M.W. $_{Cu(NO3)2.5H2O}$ = 340.32 gram/mol, M.W. $_{Cu}$ = 63.546 gram/mol

$$Cu(NO_3)_2{\cdot}5H_2O \longrightarrow CuO$$

$$\text{Mol of } Cu(NO_3)_2{\cdot}5H_2O = \text{ Mol of Cu}$$

$$\frac{\text{Mass of } Cu(NO3)2.5H2O}{340.32 \text{ gram/mol}} = \frac{\text{Mass of Cu}}{63.546}$$

$$\frac{\text{Mass of } Cu(NO3)2.5H2O}{340.32 \text{ gram/mol}} = \frac{5.15\times10^{-4}\text{gram}}{63.546 \text{ gram/mol}}$$

Mass of $Cu(NO_3)_2 \cdot 5H_2O = 2.75 \times 10^{-3}$ gram

Calculation for energy band gab

Tauc plot was used to calculate energy band gab. Absorbance value of other wavelength was analyzed UV-visible (absorbance function). α was calculated form Absorbance value (in equation 2.6,d = 1cm) and hf value was calculated in equation A-1.All value with Tauc plot as shown in Table A-1

$$hf = 1240/\lambda \text{ (nm)} \qquad \text{Equation A.1}$$

Table A.1 All value for Tauc plot

Wavelength (nm)	Absorbance	a (cm^{-1})	hf (eV)	$(ahf)^2$ ($cm^{-1}eV)^2$
800	0.833	1.20048	1.55	3.462369
799	0.834	1.199041	1.55194	3.462723
798	0.835	1.197605	1.553885	3.463097
797	0.837	1.194743	1.555834	3.455221
796	0.838	1.193317	1.557789	3.455646
795	0.838	1.193317	1.559748	3.464345
794	0.839	1.191895	1.561713	3.464802
793	0.84	1.190476	1.563682	3.465281
:	:	:	:	:
254	0.872	1.146789	4.88189	31.34317
253	0.87	1.149425	4.901186	31.73685
252	0.868	1.152074	4.920635	32.13682
251	0.866	1.154734	4.940239	32.54319
250	0.864	1.157407	4.96	32.9561

Finally, Graph $(ahf)^2$ vs hf was created and was written linear line form stable slope point to x plot as shown in Figure A-1

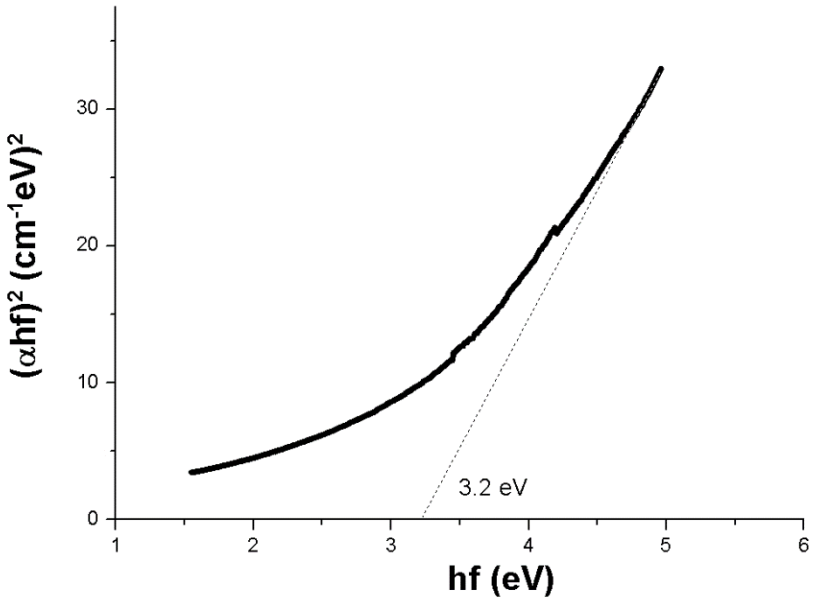

Figure A.1 Tauc plot of 40%wt TiO_2/rGO

EPA 308 method

Ethanol standards for injection. Prepare a series of ethanol standards by dilution with DI water**.** The column coated with polyethylene glycol (DB-WAX) was used this method. Using Helium (Ultra high purity) for carrier sample to flame ionization detector (FID) detector and using Oxygen/Hydrogen for fire with detector The following operating conditions are required for the GC:

Injector: Configured for capillary column, split less, 200 °C (392 °F).

Carrier: Helium at 10 ml/min.

Oven: Initially at 45 °C for 3 minutes; then raise by 10 °C to 70 °C; then raise by 70 °C/min to 200 °C.

Calculate for ethanol production

Data of Gas Chromatography was determined relation between Area peak and concentration of ethanol (in Figure xx)

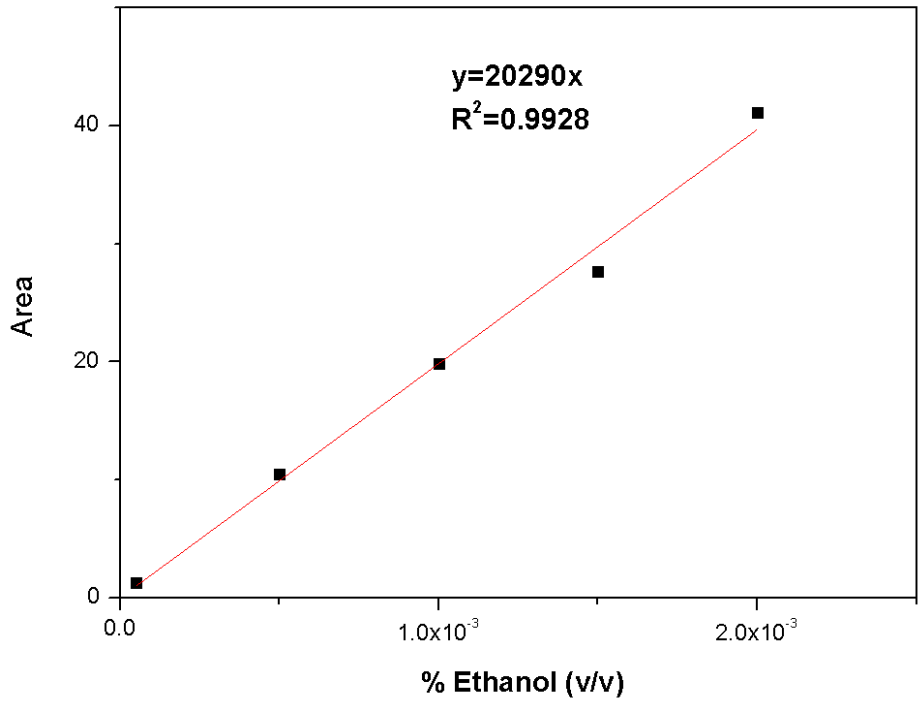

Figure A.2 Calibration curve of ethanol solution

$$y = 20290x$$

$$\text{Area} = 20290 \times \%\text{Ethanol}$$

$$\%\text{Ethanol} = \text{Area}/20290$$

In 20%TiO_2/rGO condition; Area from gas chromatography is 3.32196

$\text{density}_{\text{ethanol}}$ = 1.05 g/cm^3,$\text{M.W.}_{\text{ethanol}}$= 60.05, Mass of catalyst for reaction(g_{cat}) = 0.1 g

$$\%\text{Ethanol} = 3.32196/20290$$

$$\%\text{Ethanol} = 1.6372 \times 10^{-4}\ \%\text{v/v}$$

$$\text{Concentration (mol/L)} = (\%\text{Ethanol} \times 10 \times \text{density}_{\text{ethanol}})/\text{M.W.}_{\text{ethanol}}$$

$$\text{Concentration (mol/L)} = (1.6372 \times 10^{-4} \times 10 \times 1.05)/60.05$$

$$\text{Concentration (mol/L)} = 2.863 \times 10^{-5}\ \text{mol/L}$$

$$\text{Concentration (mol)} = \text{Concentration (mol/L)} \times \text{Volume (mL)}/1000$$

$$\text{Concentration (mol)} = (2.863 \times 10^{-5}\ \text{mol/L} \times 100\ \text{mL})/1000$$

Concentration (mol) $= 2.863\times10^{-6}$ mol = 2.863 µmol =28.63 µmol/g_{cat}

APPENDIX B

Result of gas chromatography analysis

After 12 hours of photocatalytic reaction, the liquid mixture was analyzed using gas chromatography (EPA method 308), which revealed an outstanding peak that can be indicated as ethanol.

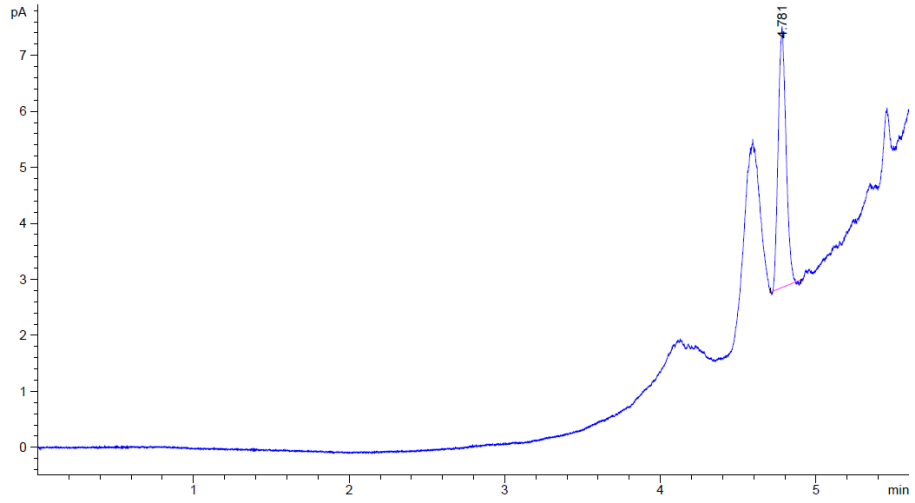

Figure B.1 Gas chromatography analysis of graphene oxide condition

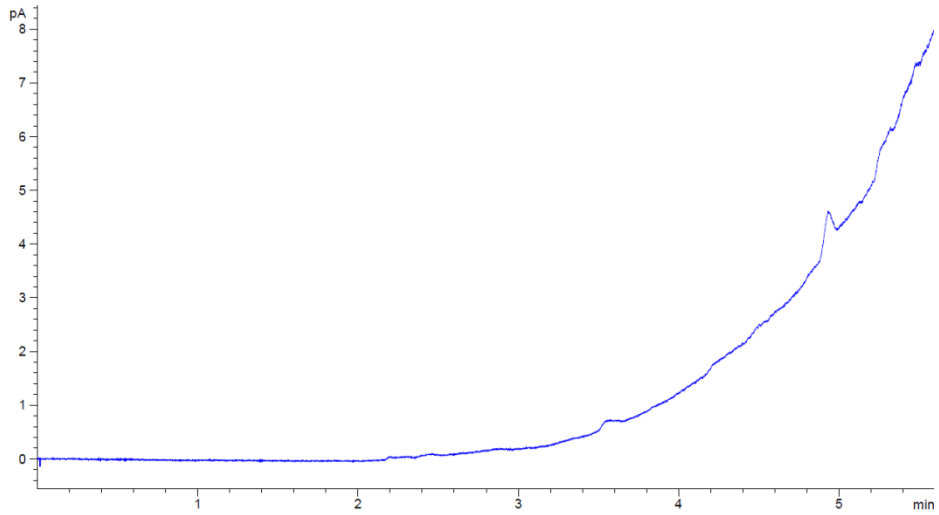

Figure B.2 Gas chromatography analysis of 10%wtTiO_2/rGO condition

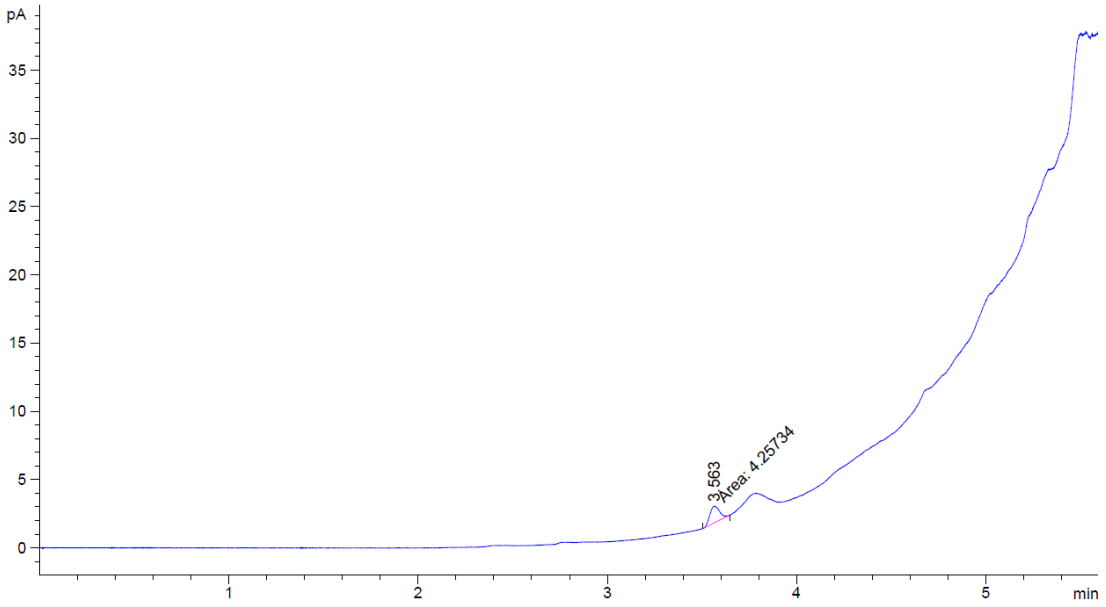

Figure B.3 Gas chromatography analysis of 20%wtTiO_2/rGO condition (Relation time = 3.553).

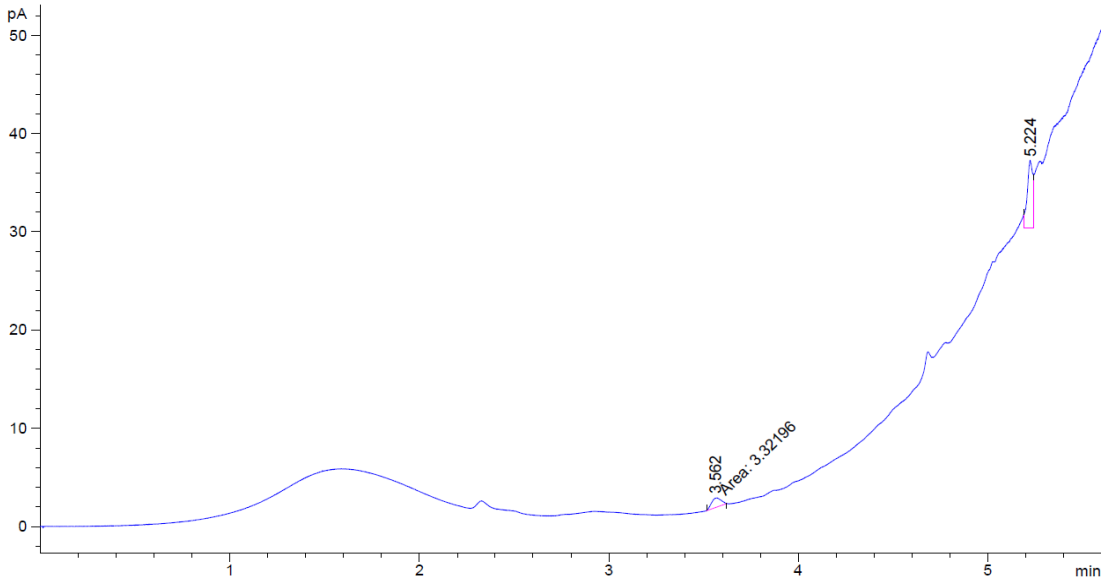

Figure B.4 Gas chromatography analysis of 30%wtTiO_2/rGO condition (Relation time = 3.562).

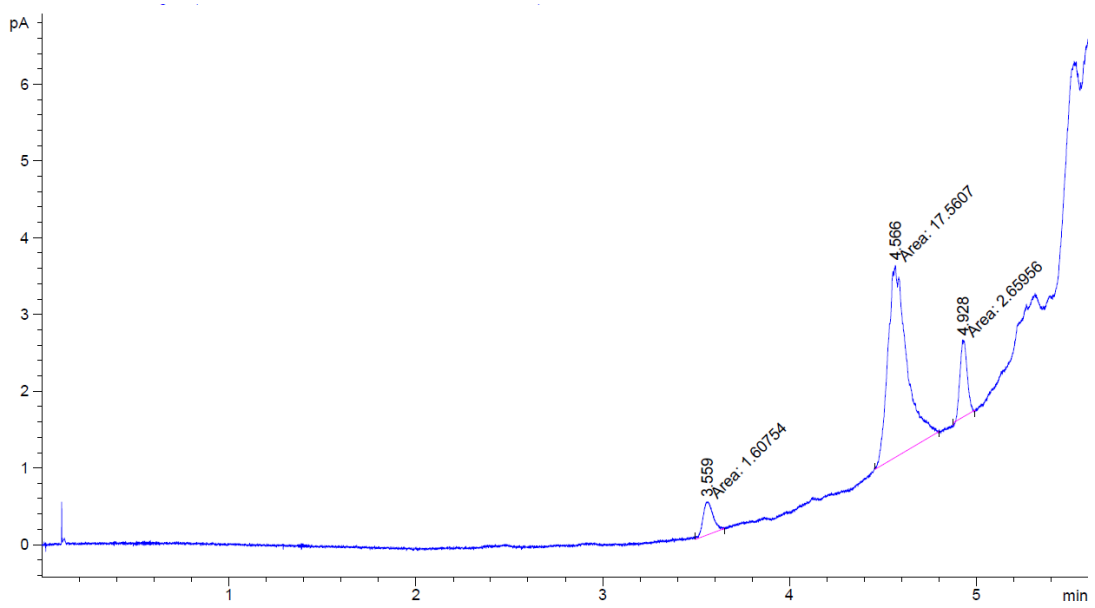

Figure B.5 Gas chromatography analysis of 40%wtTiO_2/rGO condition (Relation time = 3.559).

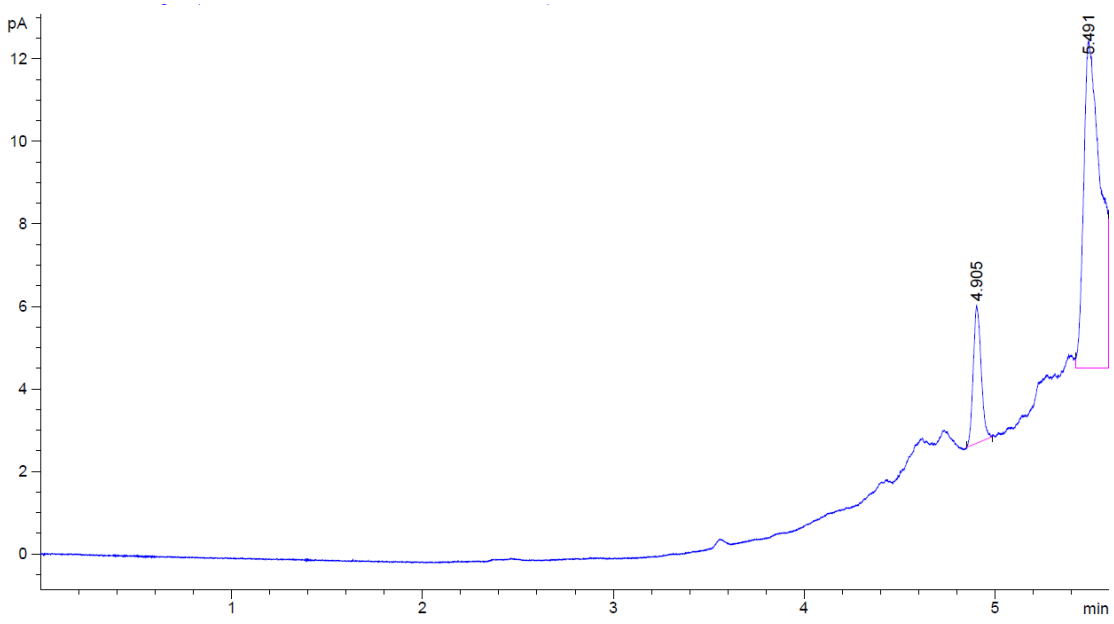

Figure B.6 Gas chromatography analysis of 50%wtTiO_2/rGO condition.

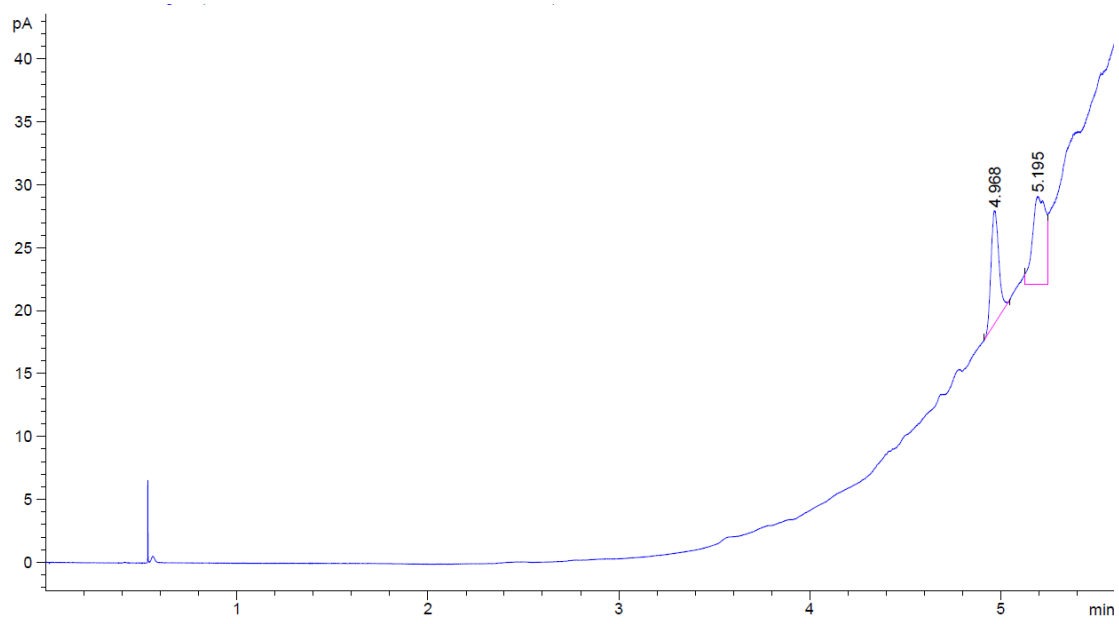

Figure B.7 Gas chromatography analysis of 60%wtTiO_2/rGO condition.

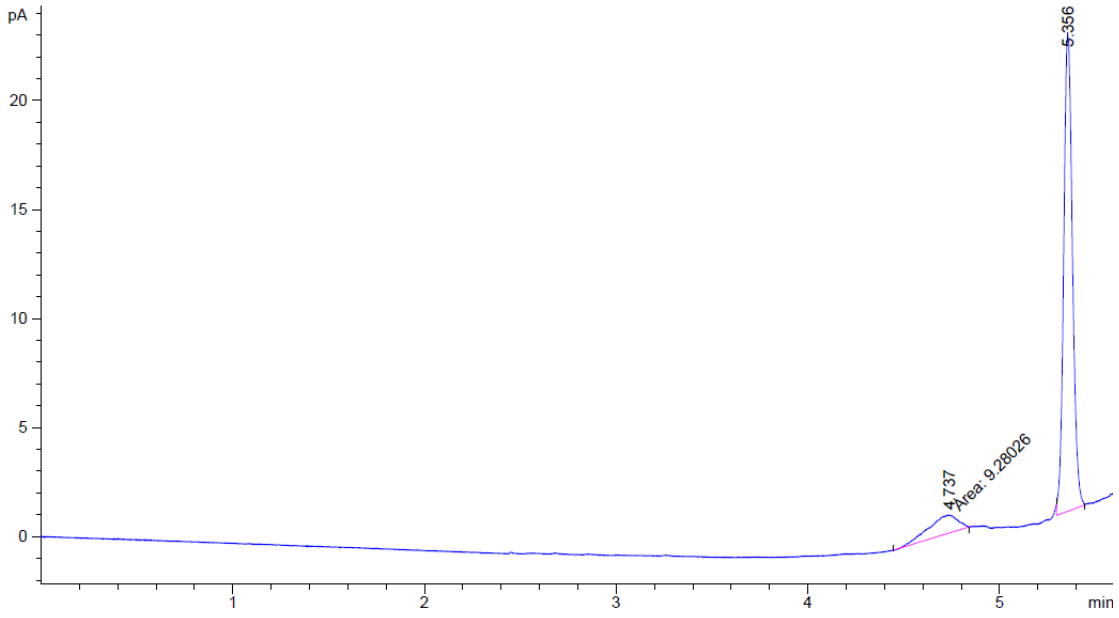

Figure B.8 Gas chromatography analysis of 0.3%wtCuO-20%wtTiO_2/rGO condition (Relation time = 4.737).

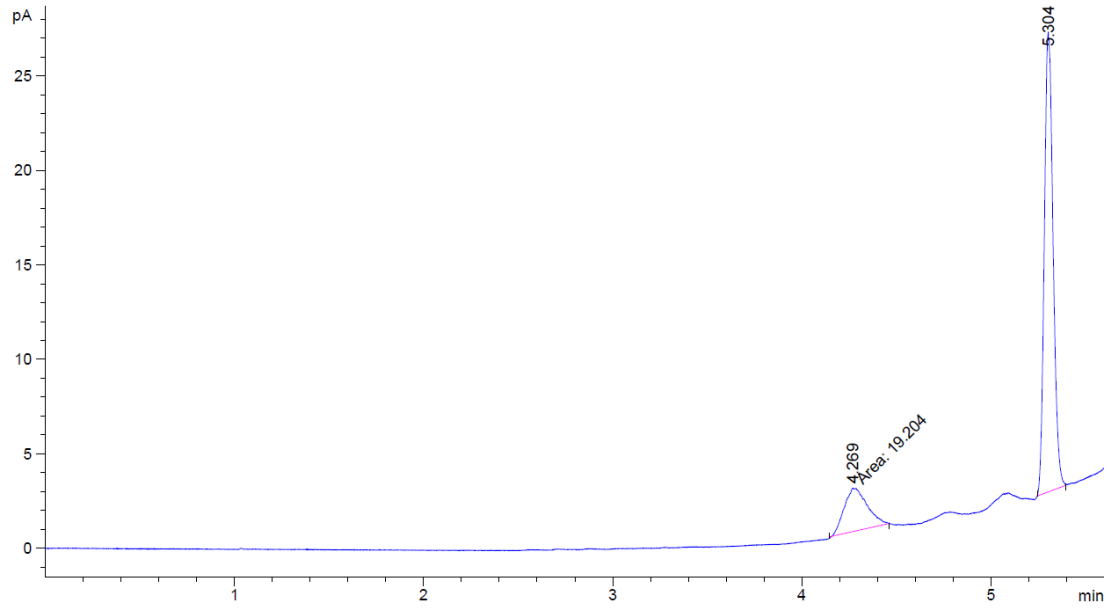

Figure B.9 Gas chromatography analysis of 0.5%wtCuO-20%wtTiO$_2$/rGO condition (Relation time = 4.269).

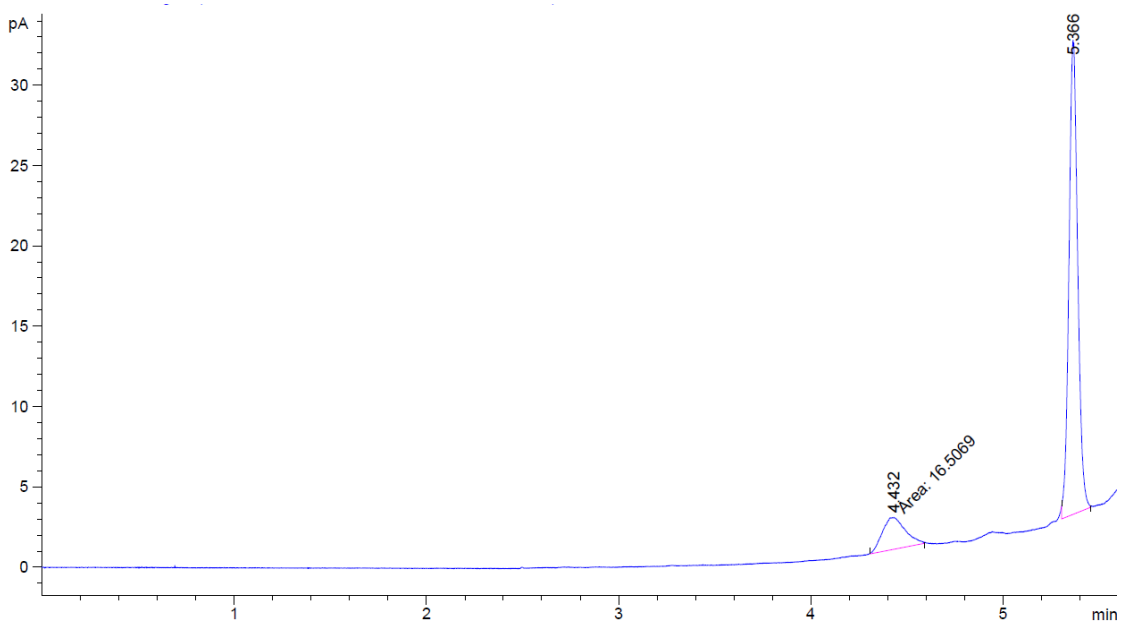

Figure B.10 Gas chromatography analysis of 1.0%wtCuO-20%wtTiO$_2$/rGO condition (Relation time = 4.432).

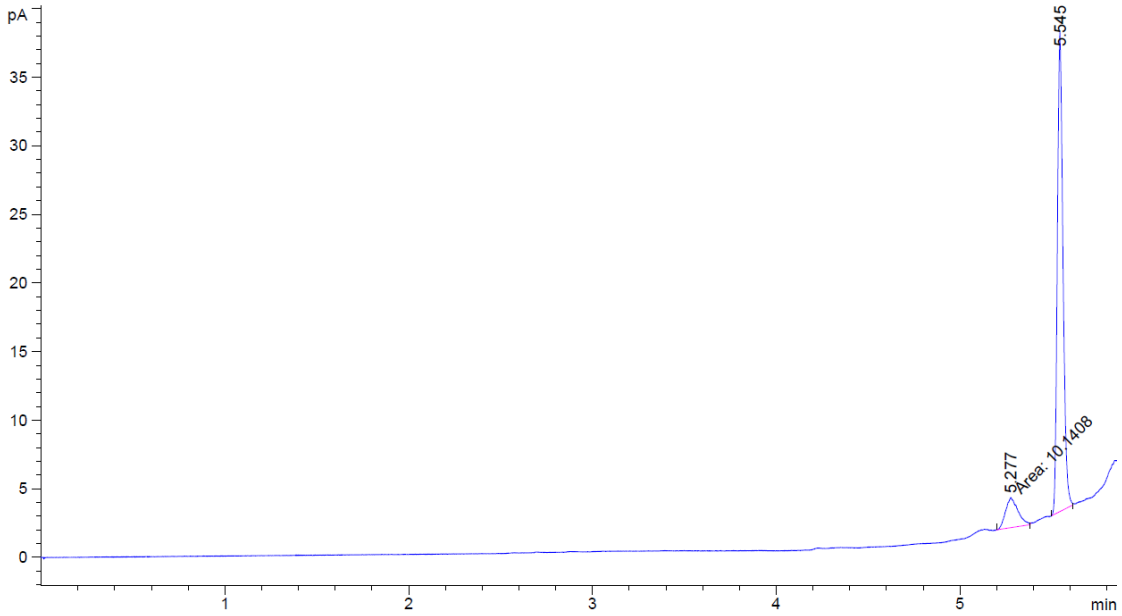

Figure B.11 Gas chromatography analysis of 2.0%wtCuO-20%wtTiO_2/rGO condition (Relation time = 5.277).

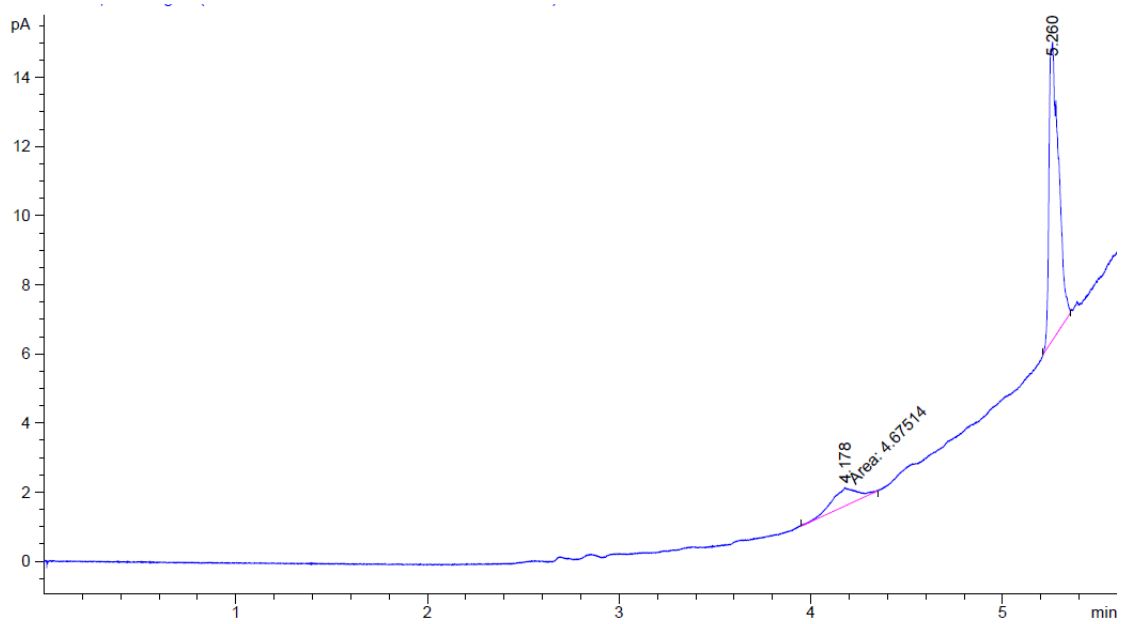

Figure B.12 Gas chromatography analysis of 0.5%wtCuO-20%wtP25/rGO condition (Relation time = 4.178)

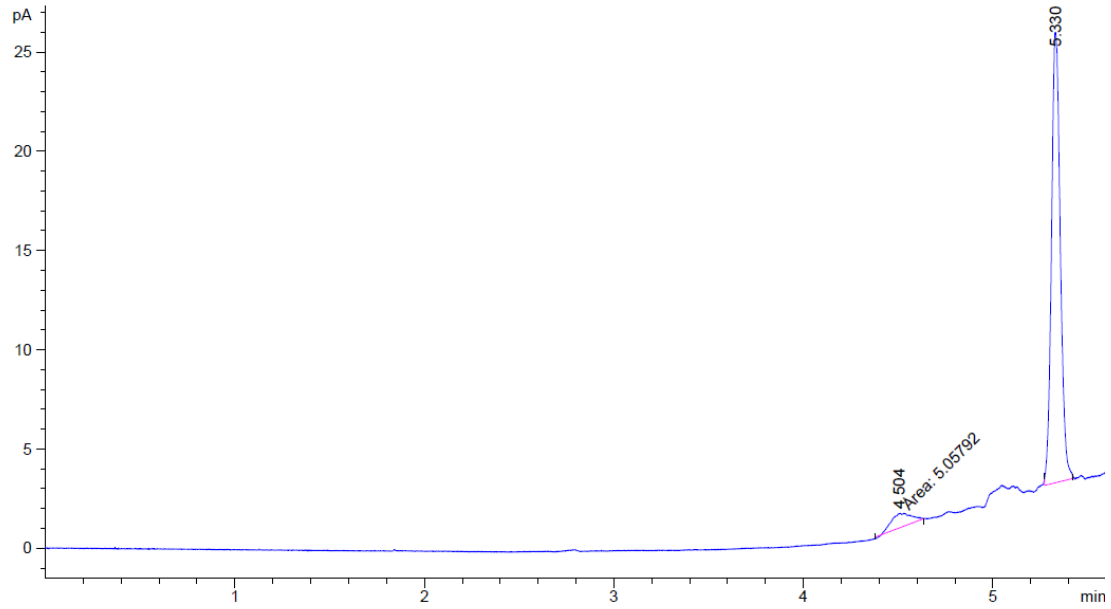

Figure B.13 Gas chromatography analysis of 20%wtP25/rGO condition (Relation time = 4.504)

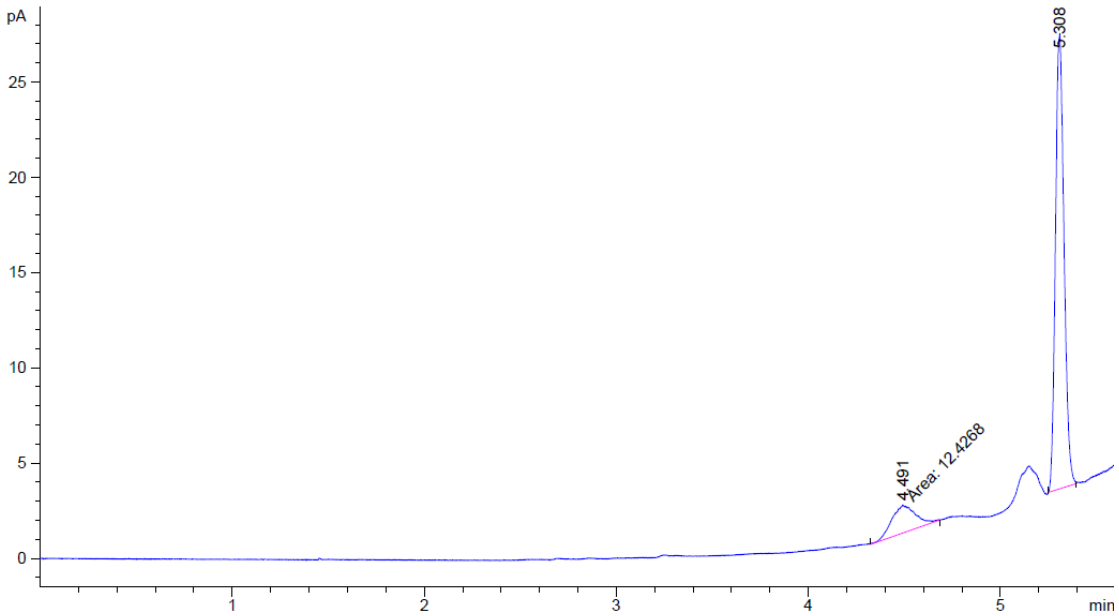

Figure B.14 Gas chromatography analysis of P25 condition (Relation time = 4.491)

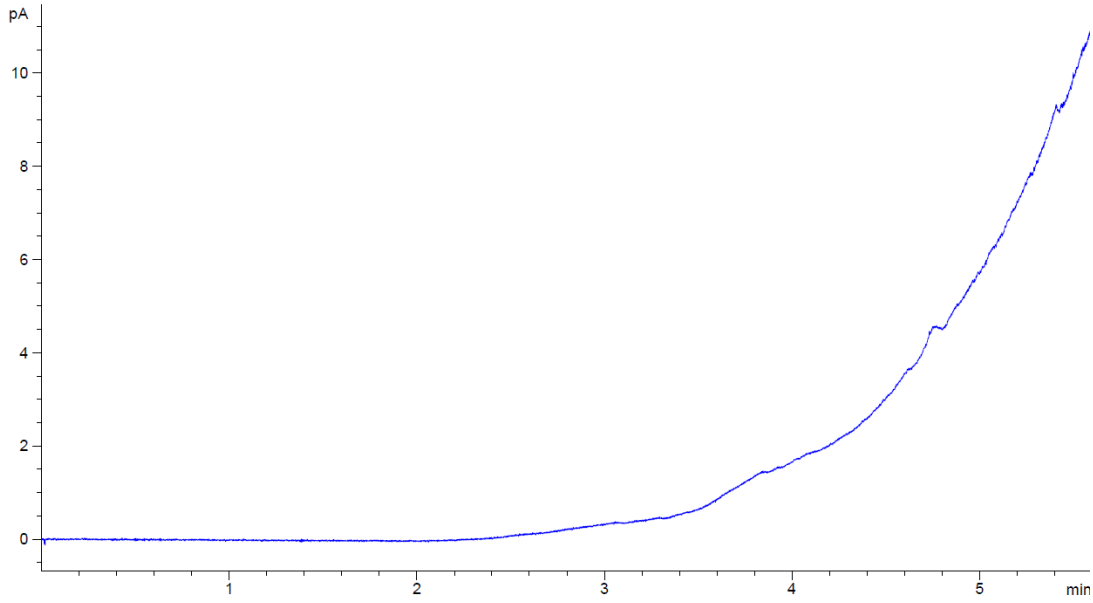

Figure B.15 Gas chromatography analysis of TiO_2 condition

BIOGRAPHY

NAME	Mr. Krittamet Yanawibut
DATE OF BIRTH	4 September 1992
PLACE OF BIRTH	Songkla, Thailand
INSTITUTIONS ATTENDED	Mahidol University, (2012-2015) Bachelor of Chemical Engineering Mahidol University, (2015-2017) Master of Chemical Engineering
RESEARCH GRANTS	Thailand Research Fund (TRF) and Research University Network (RUN)
HOME ADDRESS	22 soi 10/4 Phet Kasem Road Hatyai Songkal, 90110 Tel 094-4972200 E-mail: Krittamet.yan@student.mahidol.edu
EMPLOYMENT ADDRESS	Dept. of chemical engineering, faculty of engineering, mahidol university25/25 puttamonthon 4Rd.,Nakornpathom,7317